https://doi.org/10.5194/egusphere-2026-568
Preprint. Discussion started: 5 February 2026

Drought responses of a Norway spruce forest on drained peat soil: combining sap-flow sensors, eddy-covariance, soil and UAV data

Pavel Alekseychik[1,4], Mikko Peltoniemi[1], Raisa Mäkipää[1] Ville Tuominen[2], Tuomas Laurila[2], Hamlyn Jones[3,6] Mitro Müller[7], Evegeny Lopatin[1], Helena Rautakoski[2], Timo Vesala[4,5], Samuli Launiainen[1]

[1]Bioeconomy and Environment, Natural Resources Institute Finland, 00710 Helsinki, Finland
[2] Finnish Meteorological Institute (FMI), Climate System Research, 00560 Helsinki, Finland
[3]School of Life Sciences, University of Dundee, DD1 5EH Dundee, UK
[4]Institute for Atmospheric and Earth System Research/Physics, Faculty of Science, University of Helsinki, P.O. Box 68, 00014 Helsinki, Finland
[5]Institute for Atmospheric and Earth System Research/Forest Sciences, Faculty of Agriculture and Forestry, University of Helsinki, P.O. Box 27, 00014 Helsinki, Finland
[6]School of Agriculture and Environment, University of Western Australia, WA 6009 Perth, Australia
[7]Natural resources, Natural Resources Institute Finland, 00710 Helsinki, Finland

Correspondence to: Pavel Alekseychik (pavel.alekseychik@luke.fi)

Abstract. The summer of 2021 brought a severe drought to southern Finland. We explored how a drained boreal peatland forest responds to drought by combining a wide range of in situ monitoring and Unmanned Aerial Vehicle (UAV) remote sensing. A dataset combining eddy-covariance (EC) fluxes, sap-flow sensors, UAV mapping, soil and weather data was collected. Spruce stand reaction to drought is examined at sub-daily to seasonal time scales, and its temporal and spatial features are identified separately for a recently thinned Continuous Cover Forestry (CCF) block and a control block. Sap flow data showed that the CCF-harvested block shows greater tree resilience to high vapour pressure deficit (VPD) than the control block, likely due to the higher soil water availability during the rainless and hot period. At the same time, both the control and CCF harvest blocks had notably reduced net ecosystem exchange (NEE) and increased Bowen ratio, particularly on high VPD days. The UAV surveys indicated that trees in the CCF block tend to have higher canopy temperatures and lower Normalized Difference Vegetation Index (NDVI) than in the control block, implying their possible susceptibility to more extreme drought.

1 Introduction

Nearly 80% of the forests in the Fennoscandia region are intensively managed (Högberg et al., 2021), with Norway spruce and Scots pine being the primary species (Brunner et al. 2024). Enhancement of tree growth in the Boreal region due to higher air temperature and CO_2 concentration is possible in the coming decades (Danneyrolles et al. 2023, Wang et al. 2023), however, only within the water tolerance of the tree species (e.g. d'Orangeville et al. 2018). The projections of more frequent droughts (Hammond et al. 2022, Ruosteenoja and Jylhä 2022) makes drought resistance of Norway spruce (Picea abies) a major field of inquiry (Zhao et al. 2022),

https://doi.org/10.5194/egusphere-2026-568
Preprint. Discussion started: 5 February 2026

especially due to the cascading effect of drought stress and biotic disturbances such as insect attacks (Venäläinen et al. 2020, Jactel et al., 2011; Kolb et al., 2016).

Norway spruce cultivation in the Boreal and temperate climates is widespread, owing to its superior productivity in comparison with other industrial tree species (Pretzsch 2005). Low drought resilience of Norway spruce (e.g. Lévesque et al. 2014, Vitali et al. 2017, Schmied et al. 2023, Zang et al. 2012) is, however, expected to become an important constraining factor throwing into question the feasibility of its cultivation (Aldea et al. 2023).

Strong droughts cause sharp decline of CO_2 sink in Norway Spruce-dominated stands, as observed by the studies in Boreal and Hemiboreal Europe during the 2018 extreme drought (e.g. Lindroth et al. 2020, Krasnova et al. 2022, Mamkin et al. 2022). A meteorological classification of droughts into extreme, severe and moderate is commonly used, often defined using the Standardized Precipitation Evapotranspiration Index (SPEI) (e.g. Paulo et al. 2012). However, soil drought (low volumetric water content in the rooting zone) is not a frequent condition in the Boreal region, particularly in drained peatlands. The summers in the region are more frequently characterized by air drought, i.e. VPD exceeding a certain threshold that is commonly found to be at around 1 kPa (Oogathoo et al. 2020).

Norway spruce is an isohydric species, i.e. one strongly responding to VPD increases with stomatal closure, attempting to preserve leaf water potential at the expense of lower carbon uptake, in part due to its shallow root system (Bréda et al., 2006; Hartmann et al., 2013). This leads to suppressed photosynthesis and transpiration during drought (Ditmarová et al. 2010). VPD increase over the recent decades has decreased the growth of several Boreal tree species, and will become a stronger limiting factor in the future (Mirabel et al. 2023). The drought stress has been an increasingly important limiting factor for tree growth over the last decades (Čermák et al. 2019). Drought resilience and recovery of N. spruce are further lowered when droughts become recurrent (Schmied et al. 2023), so that the predicted increase in drought frequency (e.g. Beniston 2004) will reduce the growth of Norway spruce (Zang et al. 2012). However, the strength of drought required to cause a pronounced physiological response by is currently not well understood; moderate droughts may not produce a notable effect on trees (Zang et al. 2020), or the tree reactions may be multi-directional and uncorrelated with the known drivers (Schmied et al. 2023). When coincident with soil drought, VPD stress is more likely to lead to physiological damage (xylem tensions and embolism) (Tardieu & Simonneau 1998). However, air drought itself can cause high hydraulic stress also in the absence of soil drought (Schönbeck et al. 2022).

The exact timing and magnitude of drought response on a stand scale is typically rather uncertain because the individual trees experience and react to drought at different times. In mature trees xylem and phloem water storage can compensate the deficit of soil water for about a week, with longer times for larger trees (Čermák et al., 2007). However, large trees have been found to be either more resilient (Zweifel et al., 2001) or less resilient to drought (Pretzsch et al. 2018, Schmied et al. 2022) than small trees. Young non-dominant trees and understory have smaller internal water reserves, but also experience a more moist and dark microclimate (Zang et al. 2012, Kimmins 1987, Bréda et al. 2006), which grants protection from drought. As a result, one can expect a lag of a few days in the onset of drought reactions (stomatal closure, reduction of photosynthesis and transpiration, drop in leaf potential) between the least and most resilient N. spruce trees in a stand. Moreover, these differences can also be exacerbated by the soil quality, stand structure (Schmied et al. 2022), nutrient supply and hydrology (Ovenden et al. 2021), which complicates the analysis of timing of physiologically relevant drought periods at the stand scale. There is evidence of increased resilience for Scots pine (Giuggiola et

https://doi.org/10.5194/egusphere-2026-568
Preprint. Discussion started: 5 February 2026

al. 2013) and Norway spruce stands to drought after thinning (Sohn et al. 2013). It is generally expected that thinned stands have less inter-tree competition for soil water, particularly during a drought in both Norway spruce and Scots pine (Laurent et al. 2003; Gebhardt et al. 2014, Friedrichs et al. 2009, Martín-Benito et al. 2010, del Río et al. 2017).

UAV Remote sensing has proven useful for the boreal forest research, particularly stand structure (Alderfasi and Nielsen, 2001; Erdem et al., 2010, Berni et al., 2009; Gonzalez-Dugo et al., 2012, Smigaj et al. 2024, Manase et al. 2025, Ecke et al. 2022, Hyyppä et al. 2020). However, while stand structure of typical forests of central and Boreal Europe has been explored by remote sensing (Saarinen et al. 2018, Kopačková-Strnadová 2021, Kuželka et al. 2020, Bennett et al. 2020), applications of UAV-based thermal remote sensing to tree drought stress are still rare. By 2025, a few studies had attempted UAV-borne thermography for detecting tree physiological stress (Smigaj et al. 2024). These include the thermal assessment of drought stress in beech (Krause and Sanders 2023), detection of the effect of pathogens on canopy temperature in Eucalyptus trees (Maes et al. 2018), Scots pine and Lodgepole pine (Smigaj et al. 2019) and Norway spruce (Junttila et al. 2017), mixed forest drought stress detection (Scherrer et al. 2011), thermographic assessment of drought resilience in an orchard of small black poplar (Ludovisi et al. 2017) and water-stressed apple tree identification (Gómez-Candón et al. 2016).

The objective of this study was to compare the drought responses of two adjacent stands, a recently selection-harvested and an untreated control stand, on drained peatland soil in southern Finland. The study was conducted during the non-drought year 2020, and during a long and intense drought period in 2021 likely representative of the future Boreal climate (Balting et al. 2021), which was also the year the site was selection harvested. We hypothesized that the trees in the selection harvested stand were more stressed than the trees in the unharvest control to the drought in 2021.

Difficulty to detect responses to drought in boreal forests serves as the primary premise for this work. Therefore, a diverse set of monitoring data available at the Ränskälänkorpi peatland forest harvest experiment was used to examine the possible drought responses of trees and stands. The standard ecosystem carbon, water and energy balance monitoring (eddy-covariance CO_2 and H_2O fluxes, surface energy balance, sap-flow sensors) are supplemented by thermal and multispectral UAV data. Based on these data, we conducted an overview analysis of how the drought progresses and trees respond, and compare and discuss the merits of different methods for observing drought stress of individual trees and tree stands.

2 Materials and methods

2.1 Site description

The study site is a managed fertile peatland forest Ränskälänkorpi situated north of Lahti, southern Finland (N61°11', E25°16') (Laurila et al. 2021). The site was nutrient rich forested mire before drainage conducted prior to 1960s. Additional ditches were made in the spring of 2019. Since at least 1960s and likely from an earlier date, the site developed a mixed stand consisting chiefly of Norway spruce (*Picea abies*), with smaller numbers of Scots pine (*Pinus sylvestris*) and pubescent birch (*Betula pubescens*). The oldest tree on the site whose age was measured is a 96 years old Norway spruce, implying the existence of a tree cover already in the 1920s. In a 2020, a manual inventory of 1712 trees was conducted, revealing that the dominant trees with the

https://doi.org/10.5194/egusphere-2026-568
Preprint. Discussion started: 5 February 2026

heights of over 15 m consisted of Norway spruce (73%), downy birch (15%), Scots pine (12%) and a few other species. The species were distributed evenly across the site. As the stand is Norway spruce-dominated, we focus on spruce responses at tree scale.

At the commencement of eddy-covariance (EC) and environmental measurements (winter 2019/2020), the study site represented a rather homogeneous stand (Fig. 1a). Next winter (March 2021), the stand was divided into two blocks following the main forest tracks and ditches, and the western block was selectively harvested following the practice of continuous cover forestry (CCF, Fig. 1b). The two blocks will be referred to as Control and Harvest in the following. The selection harvest led to removal of 55% of the trees over 15 m in height and reduced the projected canopy cover from 60% to 22% in Harvest block (Appendix A for details on tree canopy detection in UAV maps before and after the harvest). One-sided leaf-area index (LAI) was estimated after Härkönen et al. (2015) and Tupek et al. (2015), and was found to be 2 m^2 m^{-2} in Harvest (2021, post-CCF harvest) and 3 m^2 m^{-2} in Control.

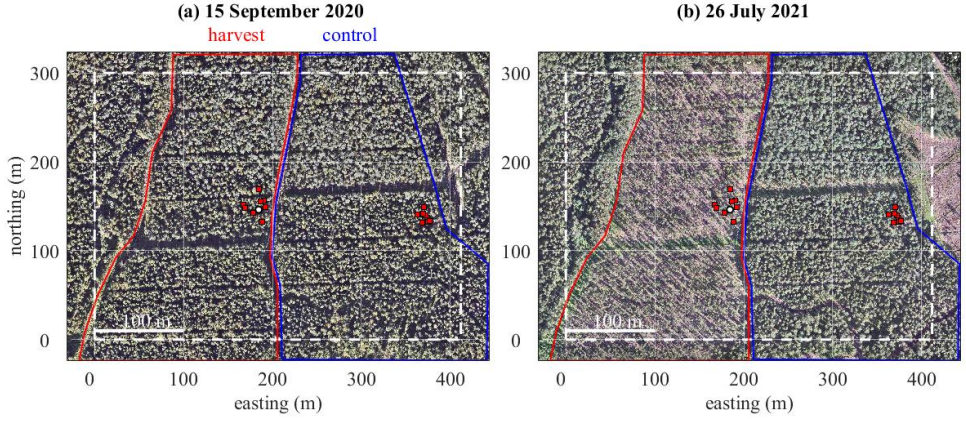

Figure 1. RGB orthophotos of the Ränskälänkorpi site before (a) and after the selection harvest (b). The primary study area of 300x400 m is shown with a white box. The ditches and the forest tracks can be clearly seen as N-S and W-E lines. The eddy-covariance tower is marked with a white square near the center of the mapped region. The trees equipped with sap flow sensors and dendrometers are shown with red squares. The boundaries of the Harvest and Control blocks are marked with red and blue lines, respectively.

2.2 Field measurement setup

2.2.1 Eddy-covariance flux measurements, gap-filling and CO_2 flux partitioning

The EC setup is mounted at a height of 29 m on a telescopic mast on the border between the selection harvested and non-harvested blocks (N61°10.973' E25°15.761'). The system consists of a sonic anemometer Metek uSonic-3 and a CO_2, H_2O gas analyzer LI-COR LI-7200RS. The raw data were post-processed using the in-house software developed by the Finnish Meteorological Institute (FMI), following the standard practices of raw

https://doi.org/10.5194/egusphere-2026-568
Preprint. Discussion started: 5 February 2026

data quality control and corrections (Aubinet et al. 2012) and the quality control of the 30-min average fluxes. The EC data in this study cover the years 2020 and 2021, without long gaps except for 26 July – 30 August 2021, when the LI-7200RS filter was clogged.

Given the position of the EC tower between the two treatments, it was necessary to separate the 30-min flux values based on wind direction. The data were considered to represent the control plot at 20°<WD<160°, and the harvest plot at 180°<WD<360°.

Since the EC data were intended to be used solely as an indicator of drought/heatwave effect on ecosystem functions, a robust modeling and gapfilling method was formulated with the purpose of obtaining time series of light-saturated ecosystem photosynthesis rate (P_{max}). The EC NEE is gap-filled by the sum of models of ecosystem respiration (Re) and photosynthesis (gross primary productivity, GPP). Nighttime Re was observed to increase exponentially at temperature range $0<T_a<10^{\circ}C$ and become invariant of air temperature at higher T_a, and is therefore modeled using a conditional function,

$$Re_{mod} = \begin{cases} Re_{ref}\ Q_{10}^{\left(\frac{T_a-10}{10}\right)}, & T_a < 10°C \\ 7.02, & T_a \geq 10°C \end{cases} \quad (1)$$

where Re_{ref} = 7.52 µmol CO_2 m^{-2} s^{-1} and Q_{10} = 4.4. The apparent Q_{10} value is slightly lower than 4.9 estimated for Norway spruce stand ecosystem respiration by Wallin et al. (2001). GPP is calculated for daytime (photosynthetically active radiation PAR > 50 µmol m^{-2} s^{-1}) as the residual of measured EC CO_2 flux and Re, and modeled as a function of PAR in two steps. In the first step, a Michaelis-Menthen function

$$GPP_{mod} = \frac{P_{max}PAR}{k+PAR} \quad (2)$$

was fit to all GPP vs. PAR data of the growing season (May-September) in order to calculate the fixed value of the parameter k = 340 µmol m^{-2} s^{-1}. Then, Eq. (2) was re-fitted to GPP vs. PAR data of each day separately so that to obtain the daily P_{max} values while k is kept constant. The variability of daily NEE and maximum photosynthesis rate P_{max} are used as proxies of an ecosystem reaction to drought.

The EC footprint was estimated using the model of Kljun et al. (2015) following Alekseychik et al. (2021a). The footprint model of Kljun et al. (2015) was solved in Matlab for each 30 min time step on a 2x2 m grid. The individual tree contributions to exchange were calculated by interpolating the georeferenced 30 min average EC footprints for the locations of the trees derived from UAV data. However, such an interpolation procedure results in a reduced footprint integral due to the number of trees being smaller than the number of nodes in the original 2x2 m footprint grid. Therefore, to preserve the integral footprint value, each individual tree footprint contribution was scaled so that to make the sum of the individual tree contributions equal to the footprint integral value outputted by the Kljun et al. (2015) code. According to this footprint calculation, the Control and Harvest blocks contributed typically 50-60% to the EC fluxes on individual days in the growing season. The rest of the EC flux was contributed by areas beyond study site, which are represented mainly by un-harvested spruce-dominated stands of varied age, except the clearcut in the eastern sector that is partly seen in the UAV maps (Fig. 1). See Appendix B for the extent of footprint and the estimation of individual tree contributions (footprint climatology).

https://doi.org/10.5194/egusphere-2026-568
Preprint. Discussion started: 5 February 2026

2.2.2 Meteorological and soil environmental conditions

Meteorological parameters were measured at the top of the 29 m tower and at ground level near by the mast. At top of the mast a radiation sensor CNR4 (Kipp & Zonen B.V., Delft, the Netherlands) was used to record the radiation balance components, from which the net radiation (R_n) was calculated. Upward- and downward-facing PQS radiometers (Kipp & Zonen B.V., Delft, the Netherlands) produced the up-and downwelling photosynthetically active radiation (PAR) and air temperature and humidity were measured by HMP155 sensor (Vaisala Oyj, Vantaa Finland). Air temperature and humidity were measured nearby by IKES Pt100 (Nokeval Oy, Nokia, Finland) and a HMP155 sensors (Vaisala), respectively, inside a radiation shield at 2 m a.g.l. Peat temperatures at the depths of 50, 20, 10, 5 and 0 cm were measured by IKES Pt100 sensors (Nokeval) and volumetric soil moisture at the depths of 20 and 5 cm by ML3 ThetaProbe (Delta-T Devices Ltd., Cambridge, UK) These parameters were collected QML201C (Vaisala) data collection board. Water table depth (WTD) was measured by Odyssey sensors (Data Flow Systems Ltd, New Zealand) in two locations in the Control block and three locations in the Harvest block; block-average WTD was used in the analysis. Precipitation was measured with a weighing rain gauge (Pluvio2, OTT HydroMet GmbH, Kempten, Germany).

2.2.3 Meteorological drought assessment

The Standardized Precipitation-Evapotranspiration index (SPEI) (Vicente-Serrano et al. 2010) was employed as a regional-scale indicator of climatological drought. A long-term time series of SPEI (1980-2021) was calculated for whole territory of Finland as follows. Daily weather data (Finnish Meteorological institute) was used as an input to SpaFHy model (Launiainen et al., 2019) to calculate the effective precipitation at the ground (liquid precipitation and snow melt) and evapotranspiration assuming LAI of 3 m^2 m^{-2} and mesic soil properties (Launiainen et al., 2022; table 2). Finally, SPEI on a 1-month timescale was calculated with the *climate_indices* Python® package using the effective precipitation and evapotranspiration. The spatial resolution of the resulting SPEI dataset is 10x10 km. Monthly SPEI values for May-September of 2020 and 2021, shown in Fig. 2, were retrieved for the Ränskälänkorpi site coordinates. Based on the classifications of McKee et al. (1993) and Paulo et al. (2012), one may interpret SPEI>0.5 as non-drought, -1<SPEI<-0.5 as mild drought, -1.5<SPEI<-1 as moderate drought, -2<SPEI<-1.5 as severe drought, and extreme drought as SPEI<-2.

The drought conditions occurring locally at the research site were assessed separately as atmospheric and soil drought, as it was expected that these conditions might show independent effects on the plants. The soil moisture threshold marking the initiation of drought stress in central and northern European conifer forest varies in previous literature as much as the definition of the drought stress itself: 0.15 m^3 m^{-3} (Galiano et al. 2017), 0.2 m^3 m^{-3} (Arend et al. 2021), 0.45 m^3 m^{-3} Kowalska et al. (2020). Soil drought was therefore defined as surface soil water content (θ_{5cm}) below 0.2 m^3 m^{-3}, as the values marking the onset of the driest period in July 2021. This value is slightly above typical wilting point of surface peat in drained forest peatlands (Menberu et al., 2021). The air drought was defined on a daily basis as daily mean atmospheric vapor pressure deficit (VPD) exceeding 1 kPa, which similarly marks high VPD stress for Boreal ecosystems (McGloin et al. 2019, Jia et al., 2016; Lasslop et al., 2010). The following analyses consider the presence of air and soil drought so defined, separately or in combination.

https://doi.org/10.5194/egusphere-2026-568
Preprint. Discussion started: 5 February 2026

2.2.4 Ecosystem-average ecophysiological drought proxies

Several quantities indicative of ecosystem reaction to drought were calculated from meteorological and EC data. The Bowen ratio BR [-] was calculated as the median ratio of sensible (H) to latent heat (LE) flux of the daytime hours (9:00-17:00).

$$BR = H\ LE^{-1} \quad (3)$$

The aerodynamic resistance to water vapour transport r_a [s m^{-1}] was calculated after Verma (1989),

$$r_a = \frac{U}{u_*^2} + \frac{\kappa B^{-1}}{\kappa u_*} \quad (4)$$

where U is the mean wind speed above the canopy, u_* the friction velocity, κB^{-1} the logarithm of the ratio between momentum and heat roughness length (Owen and Thomson, 1963), assumed to equal 2, and κ the von Kármán's constant (=0.4).

Surface resistance to water vapour transport calculated from eddy-covariance and atmospheric data ($r_{s,\,EC}$, [s m^{-1}]) was defined as (Thom 1975):

$$r_{s,EC} = r_a\left(\frac{\zeta BR}{\gamma} - 1\right) + \left(\frac{\rho C_p VPD}{\gamma R_n}\right)(1 + BR) \quad (5)$$

where ρ the air density [kg m^{-3}], R_n the net radiation [W m^{-2}], ζ the slope of the saturation vapour pressure curve [kPa K^{-1}], and C_p the specific heat of air at constant pressure [J/(kg K)]. Surface conductance $g_{s,\,EC}$ [mm s^{-1}] was calculated as a reciprocal of $r_{s,\,EC}$. Canopy water stress index was computed after Jackson et al. (1981),

$$CWSI = \frac{\gamma\left(1 + r_{s,EC}\ r_a^{-1}\right) - \gamma^*}{\zeta + \gamma\left(1 + r_{s,EC}\ r_a^{-1}\right)}, \quad (6)$$

with

$$\gamma^* = \gamma\left(1 + r_{s,EC}\ r_a^{-1}\right) \quad (7)$$

where γ is the psychrometric constant [kPa K^{-1}].

Daily ecosystem water-use efficiency WUE [g_C kg_{H2O}^{-1}] was defined using the daily integrals of GPP [g C m^{-2} d^{-1}] and ET [mm d^{-1}]:

$$WUE = GPP\ ET^{-1}, \quad (8)$$

while ecosystem light use efficiency LUE [-] was obtained as the daily integrals of GPP and PAR:

https://doi.org/10.5194/egusphere-2026-568
Preprint. Discussion started: 5 February 2026

LUE = GPP PAR^{-1}. (9)

2.2.5 Sap flow, stem diameter change and tree-level stomatal conductance from sap flow

In total, 16 spruce trees (see Appendix E) were monitored with sap flow and stem diameter sensors since June 2020 in the harvest and control blocks (8 trees in each) (Peltoniemi et al. 2023, Peltoniemi 2025, Liu et al., 2023).

The Edaphic HPV-06 sensors were installed at a height of 1.3 m on the southern side of the trees (Laurila et al. 2021), outputting the sap flow rate in the units of [l h^{-1}]. The sap flow data cover the years 2020-2021 with few gaps; however, tree No. 5 (Control block) had to be discarded due to poor data quality. Two stem diameter sensors Solartron AX-5 were installed in June 2020 for each sap-flow tree, one above the phloem and one above the xylem.

Recorded sap flow was upscaled to the plot and EC footprint scales based on the relationship between instantaneous sap flow rate and tree height (Appendix E). Tree height was chosen as the predictor of sap flow as this structural property is most readily derivable from a UAV digital elevation model (DEM).

Tree-level stomatal conductance $g_{s,sap}$ [l h^{-1} m^{-2} kPa^{-1}] was derived by normalizing the measured sap-flow of a tree (s) [l h^{-1}] by sapwood area (A_{sap}) [m^2] and VPD for the current 15 min averaging period [kPa]:

$$g_{s,sap} = s(A_{sap} * VPD)^{-1} \quad (10)$$

2.2.6 UAV data retrievals and remotely sensed indices

Spatially resolved data on individual tree parameters, including tree height, canopy area, tree canopy center coordinates, canopy temperature and colour (in RGB, NIR and Red Edge bands) were derived from imagery collected by UAV. The RGB data was used to calculate NDVI, while leaf stomatal resistance was estimated from tree canopy temperature. The UAV used to collect the remote sensing data was DJI Matrice 210 V2 with a payload of either DJI a Zenmuse XT2 thermal/RGB camera or a Micasense Altum multispectral camera.

The flights took place on four clear days (Table 1). Special ground control point (GCP) targets were designed to be easily discernible in the RGB, multispectral and thermal images alike. These were constructed as aluminum or polished steel crosses 1 m in width with a smaller cross of black duct tape marking the center. A total of 15 GCPs were used, spread evenly throughout the UAV survey zone of 20 ha.

https://doi.org/10.5194/egusphere-2026-568
Preprint. Discussion started: 5 February 2026

Table 1. The summary of UAV flights. GSD – ground sample distance of the orthomosaics.

flight No.	date	flight altitude a.s.l. (m)	capture period	T_{pool} actual; T_{pool} UAV (˚C)	Number of thermal/RGB captures (DJI Zenmuse XT2)	GSD thermal (cm)	Number of multispec. captures (Micasense Altum)	GSD multi-spec. (cm)	GSD RGB (cm)
1	15 Sep 2020	100	12:35-14:36	9.8; 5.6	2611	11.4	-	-	2.5
2	2 June 2021	100	9:44-10:29	-	-	-	1172	4.6	-
3	14 July 2021	120	16:00-18:00	-	-	-	472	5.5	-
4	26 July 2021	100	10:39-11:19	19.1; 20.0	1160	12.6	-	-	2.4

The mosaicking of RGB, thermal and multispectral images was performed in Agisoft Metashape®. The UAV multispectral and RGB data were retrieved and processed following the standard methods (Barbedo 2019, Tmušić et al. 2020), yielding RGB and multispectral orthomosaics, 3D point clouds, and digital elevation models (DEM). The resolution (ground sample distance) of the final orthomosaics is given in Table 1. The processed UAV orthomosaics are shown in Appendix F.

Thermal images were retrieved by UAV in programmed flights on 15 September 2020 and 26 July 2021, ensuring side and frontal image overlap of over 80%. A thermal emissivity value of 0.98 was used. The thermal images were processed in Agisoft Metashape®, in which the more detailed RGB point cloud was used in order to achieve better quality in the thermal orthomosaic. The ground sample distance (GSD) of the processed thermal orthomosaic was about 11.4 – 12.6 cm. The individual tree canopies were identified in the 2020 and 2021 RGB orthomosaics using a custom segmentation algorithm. For details on UAV imagery processing, see Appendix C. The canopy temperature bias related to differing levels of incident solar radiation was removed using a canopy brightness-based approach (Appendix G).

2.2.7 Temperature-based determination of tree stomatal conductance

A novel method for tree physiological stress estimation based on UAV thermal imaging was developed by adapting an approach designed originally for the use in greenhouses and laboratory experiments (Jones et al., 1992; Leinonen et al., 2006; Guilioni et al., 2008) to open forest canopy conditions. In the case of isolateral leaves and using both wet and dry leaf references, the surface temperature-based stomatal resistance can be defined as (Guilioni et al., 2008):

$$r_{sT} = \left[r_{a,w} + 2\Delta\gamma^{-1}r_{H,R}\right](T_c - T_w)(T_d - T_c) \quad (11)$$

https://doi.org/10.5194/egusphere-2026-568
Preprint. Discussion started: 5 February 2026

where T_c is the tree crown temperature, T_w the wet reference temperature, T_d the dry reference temperature and $r_{a,w}$ the boundary layer resistance to water vapour transfer [s m^{-1}], estimated as (Verma 1989):

$$r_{a,w} = 0.92 r_a. \quad (12)$$

In Eq. (11), $r_{H,R}$ is the parallel resistance to heat (r_H) and radiative transfer (r_R):

$$r_{H,R} = \frac{r_H r_R}{r_H + r_R} \quad (13)$$

$$r_R = \frac{\rho C_p}{8 \varepsilon \sigma T_a^3} \quad (14)$$

$$r_H = \frac{r_a}{2}. \quad (15)$$

The dry and wet references were constructed as two piles of spruce branches with areas of 1 m^2 and up to ca. 30 cm high lying on a frame raised 70 cm above ground on four wooden poles. Mounting the branch piles on a raised frame was intended to mimic forest canopy by ensuring better aeration of the branch piles from the bottom and thus creating a closer imitation of aerodynamic resistance to water vapor transport in a real canopy. The wet and dry references were captured by the UAV thermal camera from a ca. 40 m altitude a.g.l. just before the start of the programmed flight. The references were in direct sunlight. Immediately before being captured, one of the branch piles was sprayed with 15 liters of water from a watering can, which is therefore equivalent to 15 mm of rainfall. The dry and wet reference temperatures T_d and T_w were obtained as the mean radiometric temperatures of the two piles. Appendix D details the arrangement of the dry and wet references and water pool (reference temperature) for the correction of the mean surface temperature in the UAV thermal orthomosaic.

https://doi.org/10.5194/egusphere-2026-568
Preprint. Discussion started: 5 February 2026

3 Results

3.1 Meteorological evidence of drought

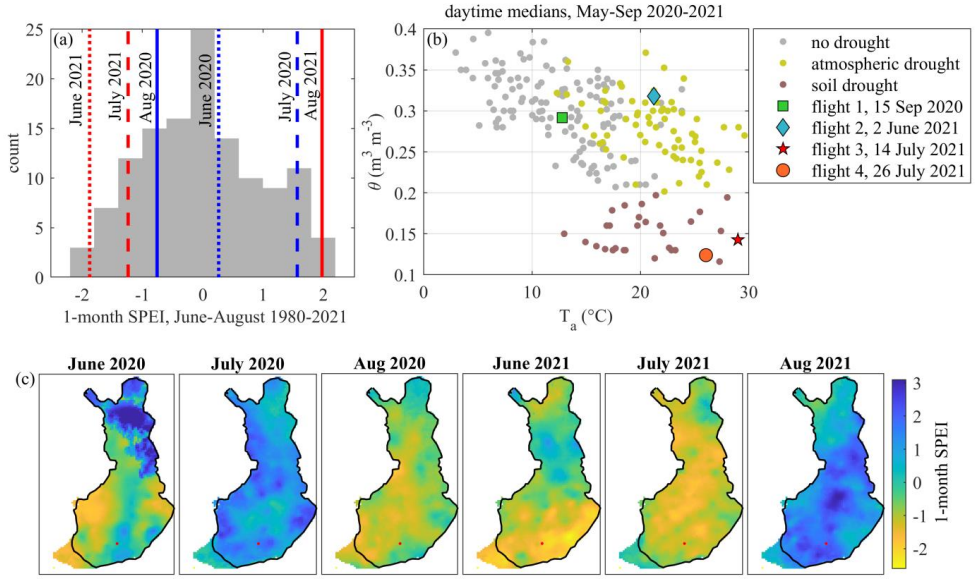

Figure 2. (a) Monthly SPEI drought index for the summer months of 2020 and 2021 for the location of Ränskälänkorpi site, with the 40-year distribution of monthly SPEI values for June-August shown with grey shading; (b) daytime median soil moisture at 5 cm depth in the Harvest block *versus* air temperature; the UAV flight days are marked with special symbols; (c) monthly SPEI distribution (negative values indicate dry conditions). The location of the Ränskälänkorpi site is marked with a red dot.

The available dataset covered two years, 2020-2021, with 2020 characterized by a warm summer without soil moisture deficit, and 2021 with a hot summer that led to a substantial drop in WTD and soil moisture. The summer of 2020 at Ränskälänkorpi site can be described as average in terms of drought index SPEI (Fig. 2a). The following year 2021 showed more extreme weather, with very dry June and July that were followed by a wet August. Note that the occurrence of dry and wet conditions in specific months varies strongly across Finland due to rainfall patterns (Fig. 2c).

Seasonal and synoptic scale weather changes can be seen as broad ranges of daily median soil moisture and air temperature (Fig. 2b). Defined using the VPD and θ threshold (Sect. 2.2.3), the days marked as "no drought", "air drought" and "soil and air drought", form distinct clusters. VPD over 1 kPa occurred at median daily temperature as low as 12.5 degrees, which is not uncommon for spring weather in the region. However, the hottest days with median daytime T_a approaching 30°C coincided with either low or high soil moisture content (range 0.12-0.37 m^3m^{-3}). Therefore, the studied forest was exposed to a range of atmospheric and soil drought conditions and their combinations during the two growing seasons.

https://doi.org/10.5194/egusphere-2026-568
Preprint. Discussion started: 5 February 2026

400 A top soil water content sensor (in the Harvest block) indicated a steep drop in the -5 cm water content during the hottest part of the 2021 drought, in late June – early July (Fig.3). The difference between the temporal courses in WTD and θ implies hydraulic decoupling between topsoil and the deeper horizons when WTD is below a certain level; this phenomenon further complicates the assessment of drought drivers and challenges the very definition of drought.

405

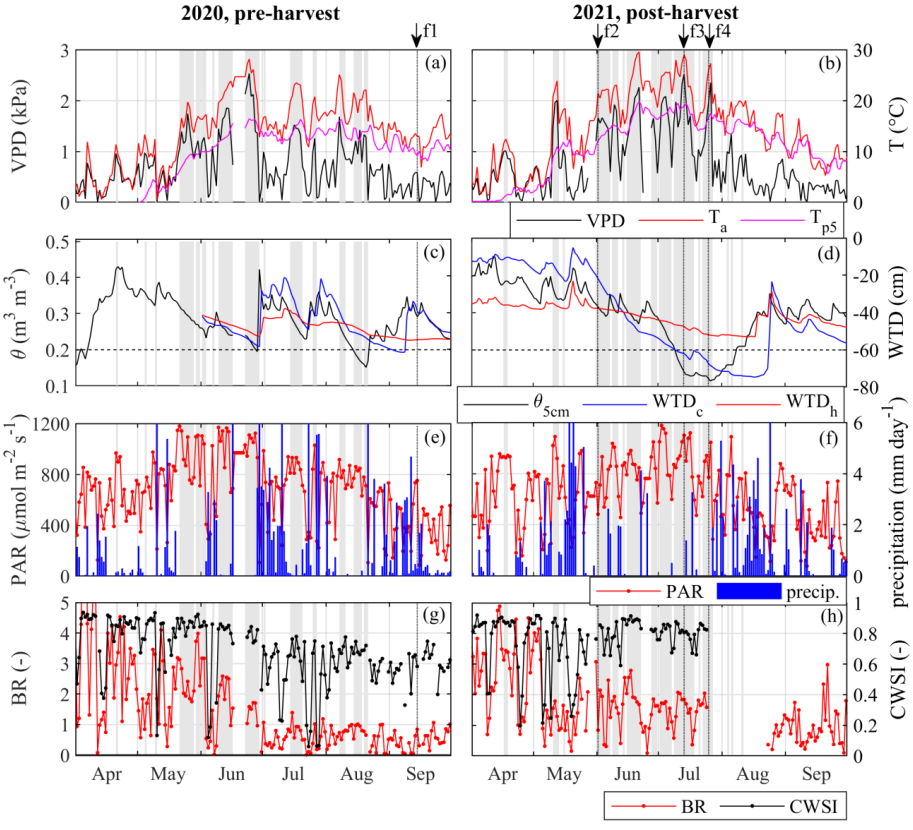

Figure 3. Daily average meteorological and soil variables. (a-b) Daytime VPD, air temperature (T_a) and 5cm soil temperature (Tp5); the grey shading here and in the following figures corresponds to days with mean VPD>1 kPa; (c-d) soil moisture θ_{5cm} at 5 cm depth and water table depth (WTD; the subscripts *c* and *h* stand for
410 Control and Harvest sectors, respectively); the value of θ_{5cm} = 0.2 defining soil drought is marked with a dotted line; (e-f) photosynthetically active radiation (PAR) and precipitation; (g-h) Bowen Ratio (BR) and Canopy Water Stress Index (CWSI). The arrows indicate the dates of the four UAV flights. The CCF harvesting was done in the early 2021, before the period shown.

415 The summer of 2020 started with rather hot and dry spell in May and June (Fig. 3a), which was brought to an end by strong rainfalls, which continued in the first half of July (Fig. 3g). Relatively wet and cool weather persisted for the rest of the summer. In contrast, 2021 received ample rainfall in May (Fig. 3g), after which ensued a hot and rainless period that lasted until the very end of July. We thus consider June and July 2021 to be

https://doi.org/10.5194/egusphere-2026-568
Preprint. Discussion started: 5 February 2026

a period of extreme drought. Persistence of such conditions led to a large drop in WTD and θ_{5cm}, particularly in July (Fig. 3d), corresponding to low SPEI (Fig. 2f-g). Of note is the WTD relation between the two blocks: WTD was higher in Control during the wet periods of 2020, but lower during the drought of 2021 (Fig. 3c,d). Water level decline was much steeper in Control than Harvest, which is probably due to water use by a larger number of trees remaining in Control, compared with the low-tree density CCF state of the Harvest block. It should be noted that air drought (VPD >1 kPA) was frequent, in both 2020 and 2021, which is important in view of conservative stomatal closure dynamics of Norway spruce. The Bowen ratio was approximately twice higher in June-July 2021 than in the corresponding period of 2020, with less pronounced but similar differences in canopy water stress index (Fig. 3 g,h), which could be a result of both the smaller number of trees in the post-harvest year 2021 and the drier conditions of June-July 2021. The CWSI averaged 0.8 in the drought periods. The summer of 2021 was also generally sunnier than that of 2020 (Fig. 3e,f).

3.2 Eddy-covariance CO_2 fluxes, WUE and LUE under drought

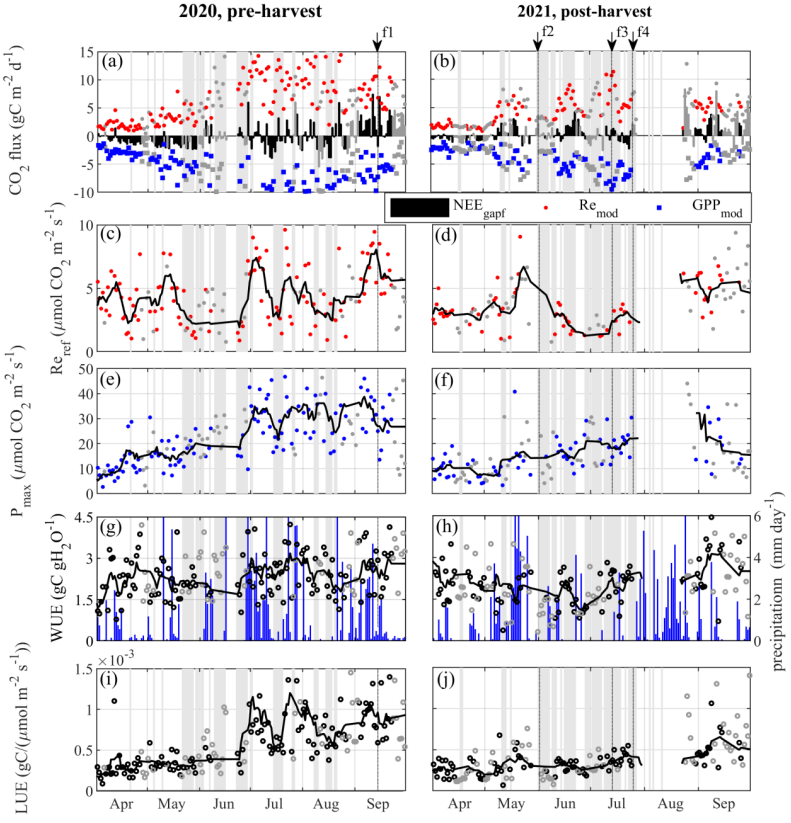

Figure 4. (a,b) daily NEE, Re and GPP; (c,d) reference respiration Re_{ref}; (e,f) light-saturated photosynthesis P_{max}; (g-h) water use efficiency WUE; (i-j) light use efficiency LUE. The UAV flights are marked with arrows

https://doi.org/10.5194/egusphere-2026-568
Preprint. Discussion started: 5 February 2026

f1-f4. The shading is for the periods of VPD > 1 kPa. The coloured markers (a-f) and black markers (g-j) show the days of easterly wind (from the Harvest block), while the grey markers correspond to easterly winds (from the Control block). The smoothing averages (black bold lines) are calculated only using the days with the winds from the direction of the Harvest block.

The growing season (April-September) NEE, GPP and Re (Fig. 4a,b) illustrate two major points. Firstly, there is an apparent drop in the absolute values of NEE and component fluxes Re and GPP in 2021 compared to 2020, which reflects the effect of selection harvesting (see also Fig. 5). This reduction in CO_2 exchange rates is also apparent in the reference respiration rate (Re_{ref}) and ecosystem photosynthetic capacity (P_{max}, Fig. 4c-f), and in the light use efficiency (Fig. 4g-j).

Secondly, the fluxes and bulk ecosystem parameters exhibit fluctuation at a weekly to seasonal timescale governed by phenology and weather changes. Rainy periods are followed by increased photosynthesis and respiration rates, as seen in Re_{ref}, P_{max} and LUE, while the high-VPD periods cause respective reductions. The two main rainy periods on record showing this dynamic are late June - early July 2020 and mid-May 2021. Overall, the correlations with VPD were more pronounced in 2020 than 2021, likely due to the higher number of trees before the harvest, and the stronger 2021 drought.

The temporal variability of CO_2 exchange parameters is remarkable during the dry period of 2021. Re_{ref} and P_{max} and LUE were at low values in the early June when the drought began, and afterwards showed a steady increase until late July. This dynamic is likely mostly governed by the normal seasonality of boreal Norway spruce stands. At the same time, WUE oscillated widely during the period without apparent correlation with the other quantities. It is noteworthy that WUE clearly increased in late July 2021 during the peak drought.

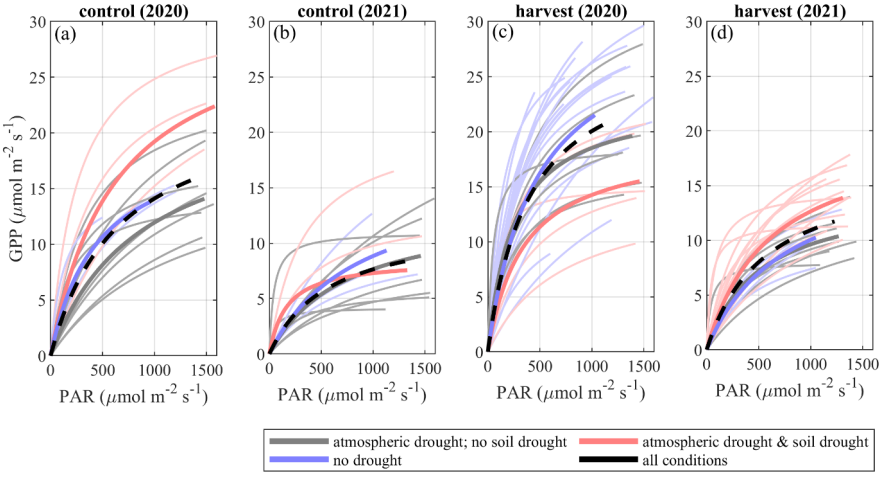

Figure 5. Light response curves for individual days in June-July of 2020 and 2021. (a) control, 2020; (b) control, 2021; (c) harvest, 2020; (d) harvest, 2021. The bold curves are the light response curves calculated from the mean of the P_{max} and k parameters of the individual days in the respective drought classes. The black dashed lines show the mean light response curves calculated for all conditions.

https://doi.org/10.5194/egusphere-2026-568
Preprint. Discussion started: 5 February 2026

The photosynthetic light response curves of June-July (Fig. 5) reveal wide differences between the control and harvest blocks. First of all, the photosynthetic efficiency, which can be interpreted as GPP at very high PAR was lower in 2021 than in 2020 in both blocks. In turn, the Harvest block photosynthetic efficiency was higher than that of the Control block in both years, both before and after the CCF thinning. The data for the Control block contains a limited number of days with soil drought, so that one can only infer that P_{max} at no drought is close to the curve representing the overall mean conditions (Fig. 5a,b). In Harvest, the effect of atmospheric drought seems to differ between 2020 and 2021 (Fig. 5c,d). In 2020, atmospheric drought caused a small decline in photosynthesis, while soil drought seems to have a large negative added effect (Fig. 5c). On the contrary, the 2021 light response curve at no drought on the c shows a lower P_{max} that the curve at atmospheric & soil drought (Fig. 5d).

It is of note that the drought periods are always associated with more sunlight than at mild weather, which is clear from the extent of the light response curves along the x-axis. Even when the drought effect on light response curve is apparent, e.g. in Harvest in 2021, the higher amount of sunlight at drought at least partly compensates for the lower P_{max}, leading to a similar value of the integrated GPP as at no-drought conditions.

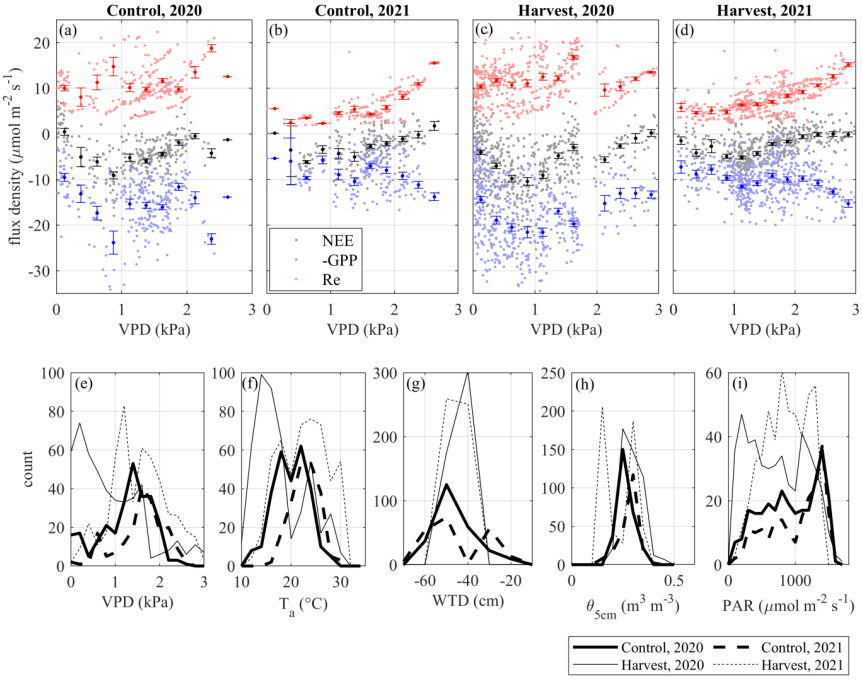

Figure 6. (a-d) Daytime 30-min averages of net ecosystem exchange (NEE), gross primary productivity (GPP) and ecosystem respiration (Re) model *versus* vapor pressure deficit (VPD). The data from June-July 2020 and 2021 are shown. (e-i) Distributions of the primary environmental drivers VPD, T_a, WTD, θ_{5cm} and PAR.

Fig. 6 shows the dependency of daytime NEE and its components on VPD over the two growing seasons. First, one must note the smaller GPP, Re and NEE in 2021 than in 2020. Regarding the relation with VPD, the

https://doi.org/10.5194/egusphere-2026-568
Preprint. Discussion started: 5 February 2026

primary feature in both blocks and in both study years is the peak NEE that is achieved at VPD of about 1 kPa. The NEE becomes smaller by modulus at drier conditions, eventually reaching zero at VPD of approximately 2 kPa, on both blocks and both years. However, the way this trend is realized in GPP and Re seems to differ between 2020 and 2021. In the dry 2021, both GPP and Re increase with VPD, where the increase in Re at VPD > 2 kPa is steeper, leading to near-zero NEE. This is not observed in 2020 as the component fluxes are more stagnant, or even reduced by modulus at high VPD.

The distributions of the primary environmental drivers for June-July periods of 2020 and 2021 (Fig. 6e-i) suggest systematic and considerable differences in the weather and soil conditions, which is of importance for the understanding of the EC fluxes. It follows that when the EC measured the Harvest block, the weather was on average cloudier and cooler, leading to low VPD stress, compared to periods of Control wind directions. The distributions demonstrate that both blocks were hotter and drier in 2021 than in 2020. The 2021 bimodality of WTD and θ in Control and Harvest reflects the rapid decrease of soil water content during the dry spell (Fig. 3).

3.3. Sap-flow and evapotranspiration under drought

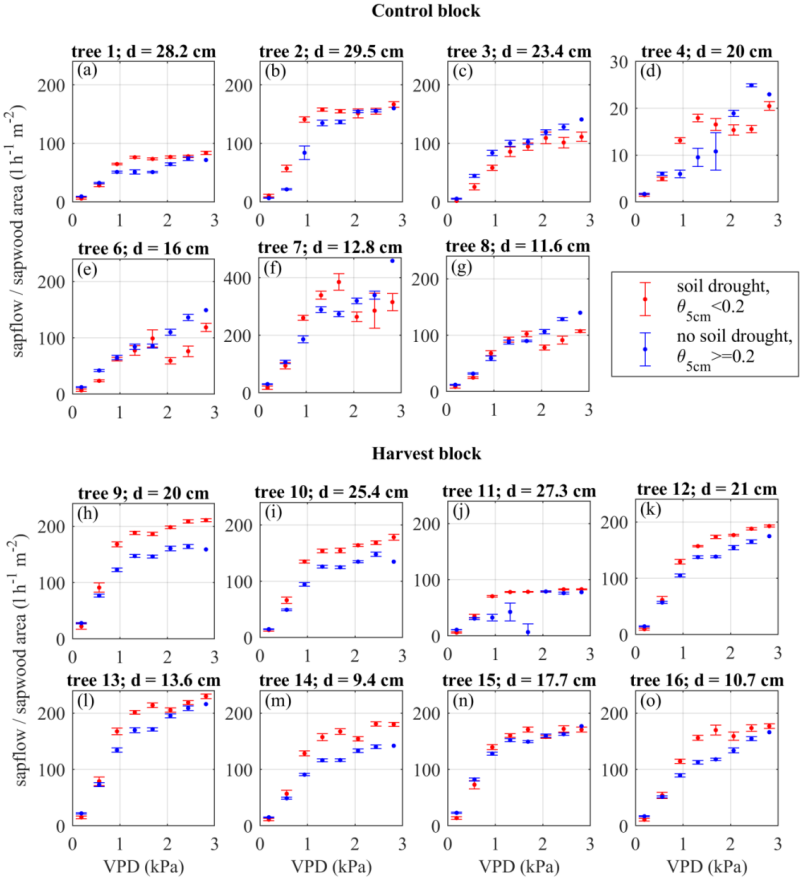

Figure 7. Individual tree sap flow normalized by sapwood area *versus* VPD in the summer of 2021. Note that the x-axis limit is 250 for all trees except 4 and 7.

https://doi.org/10.5194/egusphere-2026-568
Preprint. Discussion started: 5 February 2026

505 The sap flow data shows clear signs of VPD stress-induced limitation in tree water use, which magnitude differs between the trees and treatment blocks (Fig. 7). The most usual observed dynamic is the linear increase of sap flow with VPD up to 1 kPa, and a saturation at higher VPD, indicative of the decrease of tree-level stomatal conductance with increasing VPD. The saturating behavior of sapflow – VPD response is overall stronger during soil drought, however the slope at VPD >1 varies between the trees (Fig. 7).

510 The trees of the Harvest and Control blocks respond differently to drought. The Control trees generally show similar or lower sap flow at high VPD between soil drought / no-drought conditions. The Harvest trees, however, show higher sap flow than the Control trees throughout the VPD range.

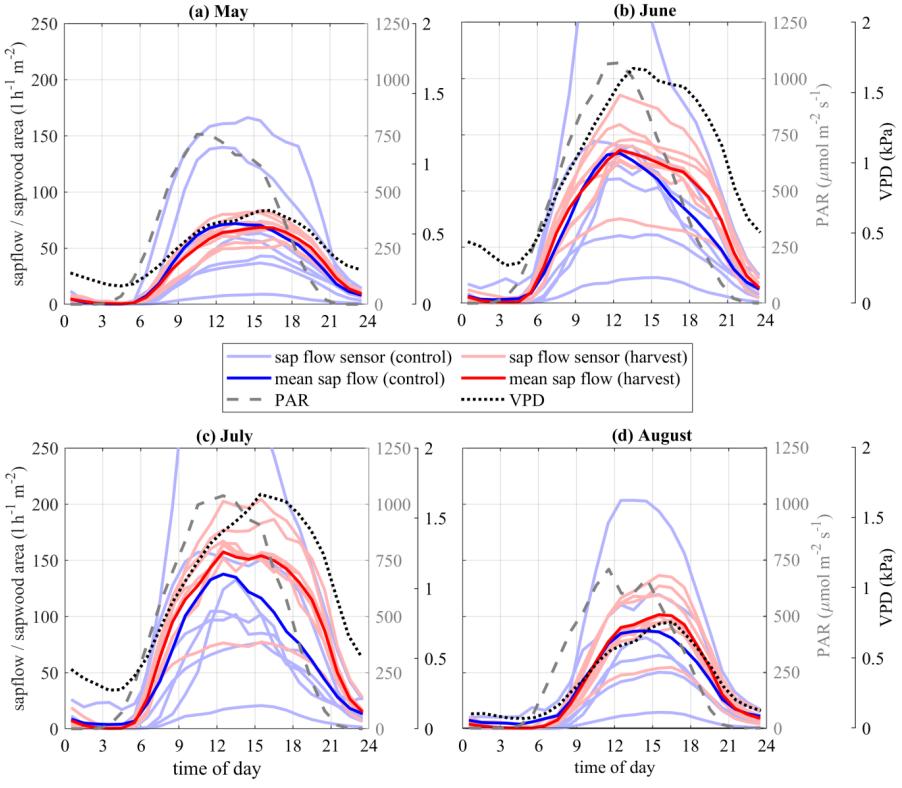

515

Figure 8. Diurnal variation of sap flow normalized by sapwood area, averaged for the months May-August of 2021. The individual tree sap flow curves are shown with pale lines (red – harvest; blue – control), while the means of all trees in both blocks is shown with bold lines; PAR is shown as a dashed line and VPD with a dotted line.

520

The diurnal cycle of sap flow closely matches the phase of VPD but lags PAR by about 3 hours (Fig. 8). The range of midday sap flow is much broader among the trees in the control than in the harvest block, which might be related to more variable light availability and soil moisture due to the denser canopy.

https://doi.org/10.5194/egusphere-2026-568
Preprint. Discussion started: 5 February 2026

In May 2021 (Fig. 8a), sap flow in control and harvest blocks is nearly identical, but June a clear afternoon dip occurs in the Control block (12-21 PM); this dip gets progressively deeper in July, and then mostly disappears in August. The timing of this relative sap flow deficit coincides with the peak daily VPD levels.

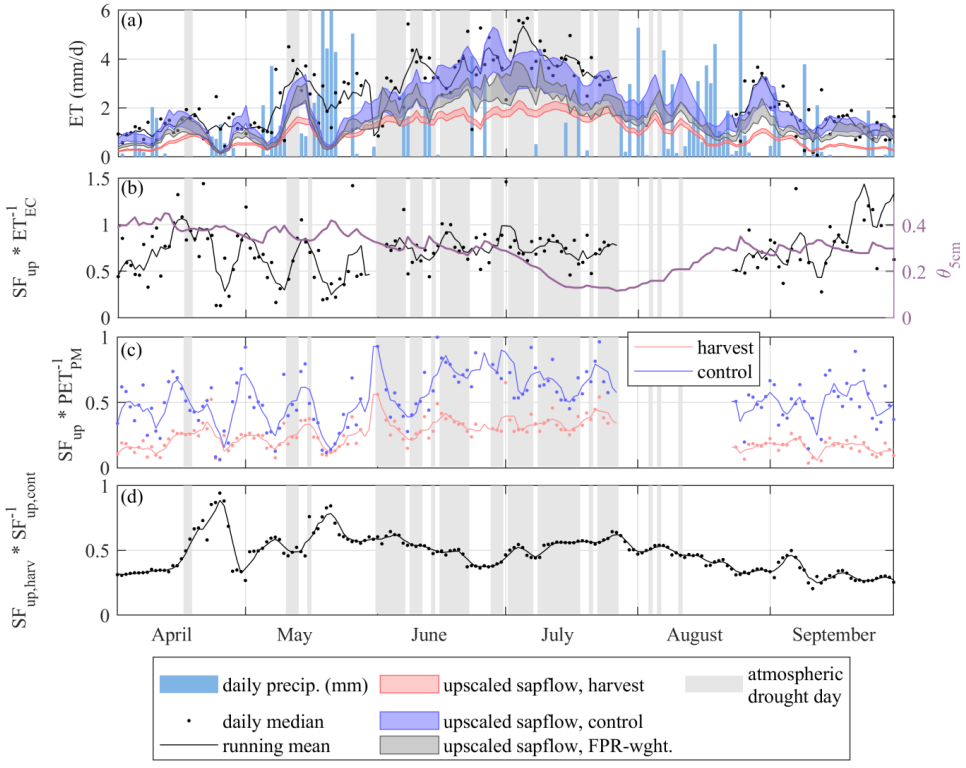

Figure 9. (a) upscaled daily sap flow given as the average of Harvest, Control blocks and as a EC footprint-weighed value; daily EC evapotranspiration (ET) is given as black dots and its weekly running average as a black line; (b) ratio between the upscaled footprint-weighed sapflow (SF) and EC evapotranspiration (c) ratio between the upscaled footprint-weighed sapflow and the Penman-Monteith potential evapotranspiration, separately for the Control and Harvest blocks; (d) ratio between the upscaled sap-flow of the harvest block and control block; (e) ratio of stomatal conductance between the small and large trees. The days of VPD > 1 kPa are marked with grey shading, as elsewhere. Daily precipitation is shown in (a) and the 5 cm soil water content in (b).

The seasonality of upscaled sap flow, representing tree stand transpiration rate, closely mirrored that of the EC evapotranspiration (ET) in 2021 (Fig. 9a), with an increase towards late June and fall off starting from July. The synchronicity between EC ET and upscaled sap flow is best seen during the ET peaks in the first half of May and late August when the canopy is dry and transpiration a major contribution to ET. However, during and following heavy rainfall events the upscaled sapflow is less than half of the EC ET; in these conditions, non-stomatal water sources in the form of interception, evaporation and forest floor evaporation constitute a major

https://doi.org/10.5194/egusphere-2026-568
Preprint. Discussion started: 5 February 2026

part of the ET. The mean ratio between the upscaled sap flow and EC ET (Fig. 9b) is 0.7. The highs in the ratio during June-July appear to occur in the periods of atmospheric drought.

There is a wide separation between the curves for Control and Harvest upscaled sap flow, reflecting the difference in tree density and leaf-area index (LAI). The footprint-weighed upscaled SF shows intermediate values as it includes fractions of Harvest and Control blocks at all times (Appendices B, E).

The upscaled block-wise sap flow normalized by the Penman-Monteith potential evapotranspiration (Fig. 9c) shows stronger dynamics at the denser Control block than at the Harvest block, most likely due to different partitioning of ET between transpiration and evaporation. There was a moderate but noticeable drop in the mean level of that quantity between the second half of June and the whole July.

3.4 UAV surveys: individual tree NDVI and canopy temperature

The previous sections used continuous in-situ observations to reveal tree and ecosystem level responses to atmospheric and soil drought. The use of UAV-based thermal and RGB images then provide snapshots to high-resolution spatial variability within and across the Harvest and Control blocks (Fig. 10). The general feature in Fig. 10 is the contrast between the spatial distributions of canopy mean vegetation index values between the surveys in non-drought (15 September 2020, 2 June 2021) and drought conditions (14 and 26 July 2020; Fig. 3), with extra effects caused by the selection harvest. The post-harvest and drought survey of 2021 shows a considerable difference between the Harvest and Control blocks that wasn't seen in the reference survey in 2020 (Fig. 10a,b). This difference is seen yet clearer in temperature-based tree crown-level stomatal conductance (Fig. 10 c,d). Higher drought-period temperatures in the Harvest block (and some of the major forest tracks in the Control block) lead to markedly higher g_{sT} estimates on average. A similar picture is revealed by the distribution of canopy brightness (Fig. 10 e,f), indicating that the trees in the Harvest block were exposed to higher visible radiation intensity. The canopy NDVI was more equal between Harvest and Control in the pre-drought survey of 2 June 2021 than in the peak drought survey of 14 July 2021 (Fig. 10 g,h). However, the mean Harvest tree NDVI was lower than that of the Control already on 2 June 2021, pointing at possible post-CCF harvest effects and different contribution of crowns vs. ground pixels in the drone images. This difference further increased by the time of the next survey on 14 July 2021, with the mean Harvest NDVI going down and the mean Control NDVI going up; the latter is likely due to typical phenology of boreal coniferous forests (Karkauskaite et al. 2017, Jönsson et al. 2010). Furthermore, a particular spatial feature becomes apparent in the drought survey (Fig. 10 h): rows of trees with low NDVI along the east-west forest tracks in the Harvest block, but also along some of the forest tracks in Control.

https://doi.org/10.5194/egusphere-2026-568
Preprint. Discussion started: 5 February 2026

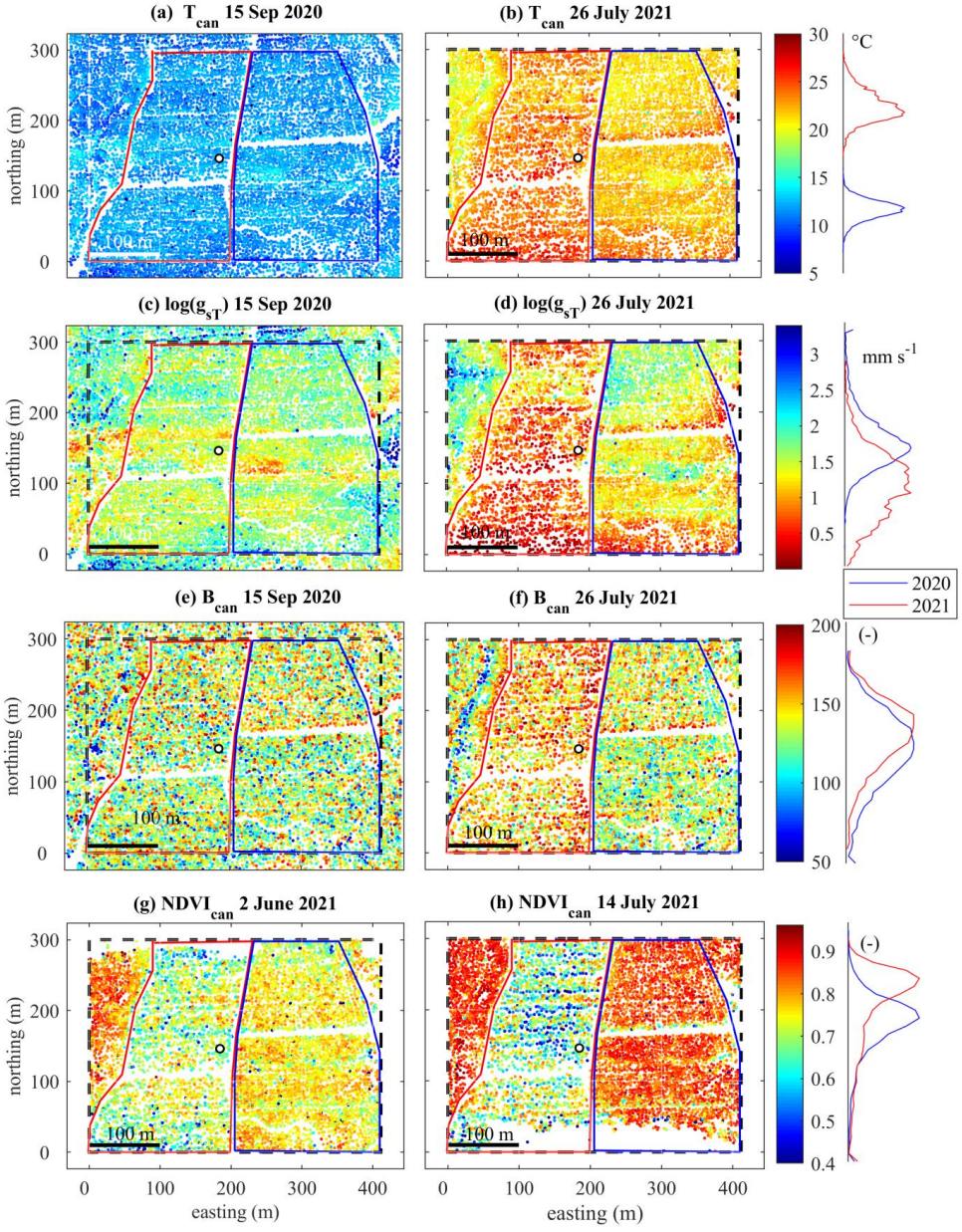

Figure 10. (a,b) tree canopy temperature in the surveys of 15 September 2020 and 26 July 2021; (c,d) logarithm of temperature-derived stomatal conductance (dates as above); (e,f) canopy brightness (dates as above); (g,h) NDVI of the trees in pre-drought conditions (2 June 2021) and peak drought conditions (14 July 2021). The plots to the right of the main panels show the tree value distribution comparisons. The boundaries of the Harvest and Control blocks are shown as in Fig. 1.

https://doi.org/10.5194/egusphere-2026-568
Preprint. Discussion started: 5 February 2026

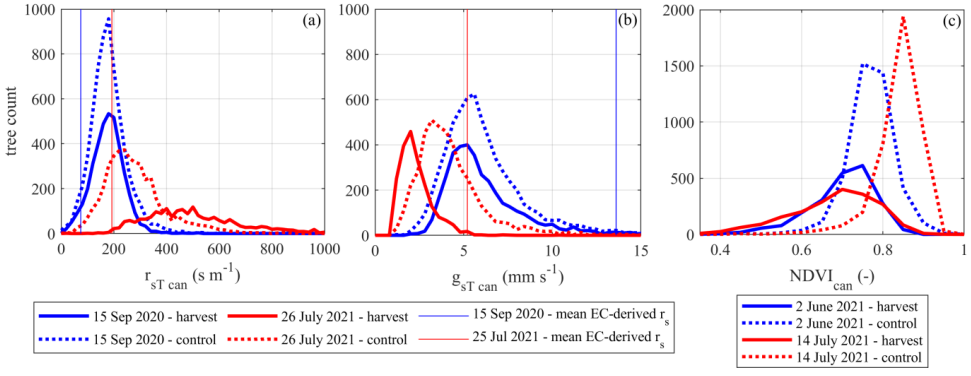

Figure 11. Distributions of individual canopy temperature-derived stomatal resistance (a) and conductance (b). The eddy-covariance resistance and conductance for the time of the respective UAV flights are shown as vertical lines.

The distributions of individual tree canopy mean thermal stomatal resistance, its reciprocal, conductance, and the tree mean NDVI at the Harvest and Control blocks are shown in Fig. 11. In the non-stress conditions, harvest and control blocks show very close distributions (the blue lines in Fig. 11) both in 2020 (before harvest) and in 2021 (after harvest). In drought stress conditions, however, significant difference emerges. The change in stomatal resistance between non-drought and drought period is stronger in the Harvest block, where the stress-day r_{sT} distribution becomes much broader than in Control. The median of surface temperature-derived tree-scale resistance is approximately twice greater than the eddy-covariance estimates for both the non-stressed and stressed conditions (and vice versa for conductance).

At the Control block, the NDVI (the mean values for individual tree canopies) in 2021 increases substantially from early June to mid-July (mean increase by about 0.1; Fig. 10 g-h & 11c). At the Harvest block, the mean or median tree NDVI did not change, but there was a definite change in the distribution shape: The number of trees with NDVI from 0.65 to 0.80 decreased, while the number of trees in the region of 0.4-0.6 increased.

https://doi.org/10.5194/egusphere-2026-568
Preprint. Discussion started: 5 February 2026

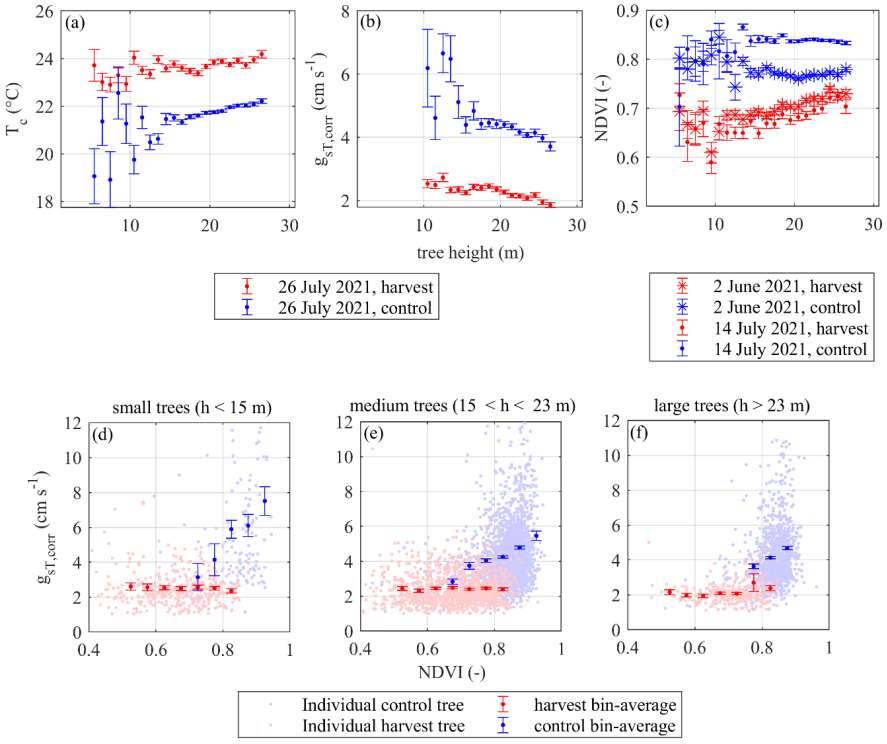

Figure 12. Tree indices plotted against tree height: (a) Canopy temperature; (b) corrected temperature-based stomatal conductance (g_{sT}). (d-f) temperature-based stomatal conductance vs. NDVI shown separately for small (d), medium (e) and large (f) trees.

Tree canopy temperature increases with tree height (and exposure to light) in both Harvest and Control, but slightly steeper in the Control block (Fig. 12a). The dependency of g_{sT} on tree height is correspondingly opposite (Fig. 12b). NDVI likewise increases with tree height, but only in Harvest (Fig. 12c), while in Control NDVI is invariant of tree height. These relationships hold both for the pre-drought and drought surveys, and the only difference between the surveys is the overall NDVI range.

The trees were partitioned into tree size groups (under 15 m, 15 – 23 m and over 23 m in height) in order to create distinct classes of small and large trees, in an attempt to improve on the practice of some previous studies that used only two classes (e.g. Zang et al. 2012). The tree mean parameters during drought (NDVI measured on 14 July and g_{sT} estimated from T imagery on 21 July 2021) show very different relationships in Control and Harvest (Fig. 12 d-f): a consistent positive correlation in Control, but essentially no correlation in Harvest. This holds for all three tree size classes.

https://doi.org/10.5194/egusphere-2026-568
Preprint. Discussion started: 5 February 2026

4 Discussion

Signs of drought stress during a hot, dry summer were detected in the carbon, water, and energy exchanges of a boreal Norway spruce-dominated forest on drained peat soil, using multiple monitoring devices. The study site consists of the selection harvesting (of continuous cover forestry CCF) and un-harvested control blocks, which were monitored using eddy-covariance, sap flow sensors and UAV surveys. We chose the approach of defining a drought with meteorological means and finding the responses at tree to ecosystem level. In meteorological terms (SPEI), June-July 2021 can be considered a severe, although not extreme, drought (Sect. 3.1, Fig. 2). The summer of 2021 represents the dry and hot conditions that have been observed in the Boreal region in a number of years over the last decades, and that will become more common in the foreseeable future (e.g. Felsche et al. 2024). The experimental setup thus has a potential to show whether a managed well-drained peatland ecosystem can show signs of physiological stress during a severe meteorological drought period.

4.1 Drought response of C and H_2O fluxes of a Norway spruce forest growing on drained peat soil

4.1.1 Photosynthetic and respiratory efficiencies in drought

The meteorological drought that occurred in southern Finland in June-July 2021 affected ecosystem CO_2 exchange and tree sap flow in the drained peatland forest. The EC CO_2 fluxes, which are primarily representative of the Harvest block, indicate that the net CO_2 sink is diminished under air drought (Section 3.2), which is manifested as the drop of photosynthetic efficiency and the actual level of photosynthesis. P_{max}, WUE and LUE indicate constrained photosynthetic capacity during the air drought periods in both 2020 and 2021 (Fig. 4). The change in vegetation functioning between the two years is readily seen as a twice lower asymptotic limit of the mean light response curve of the non-harvested block in 2021 (Fig. 5). A similar twofold drop of photosynthesis rate that was observed in Harvest is largely due to drought, with a likely compensation from selection harvesting as it increases the radiation receipt by tree crowns. Drought-induced photosynthetic efficiency loss in Norway spruce is known to be sharp, and more pronounced than that of Scots pine (e.g. Zlobin et al. 2019). Matkala et al. (2021) reported a drop in maximum photosynthesis and reference respiration in hot and dry years based on EC measurements in a Norway spruce-dominated stand. Although stronger droughts may reduce photosynthesis and the availability of carbohydrates by causing a drop in stomatal conductance and metabolic activity (Dreyer 1997, Escós et al. 2000), stomatal closure may also prevent any negative effects from mild and moderate droughts, ensuring fast recovery and continued growth (Gessler et al. 2020).

This was accompanied by declining reference respiration (Fig. 4c,d), which likewise indicates a suppression of heterotrophic respiration under drought, as observed in previous studies (e.g. Matkala et al. 2021, Lindroth et al. 2020, Krasnova et al. 2022). The lowered P_{max} and Re_{ref} led to a large decline in the mean levels of GPP and Re in June-July 2021 relative to the corresponding period of 2020 (Fig. 6).

These observations tie in with the previous studies showing the negative effects of air drought on boreal forest GPP and Re. Mirabel et al. 2023 concluded that high VPD limits the growth of typical boreal conifer species, particularly in combination with high temperature, while GPP was also found to be limited by VPD stress (Zhong et al. 2023). Granier et al. (2007) found both GPP and Re to be substantially reduced at very low soil

https://doi.org/10.5194/egusphere-2026-568
Preprint. Discussion started: 5 February 2026

water content in a range of forests of boreal and temperate European forests during the 2003 drought; Lindroth et al. (2020) report the same regarding the 2018 drought, and note that the site-mean GPP deficit correlated with the deficit in g_s in a range of boreal sites. Such negative impacts may be caused by VPD in absence of soil drought (Schönbeck et al. 2022).

The NEE shows a peak at VPD of about 1 kPa, and a decline at stronger air drought (Fig. 6). A substantial fraction of this deficit may be contributed by ground vegetation that is less resilient to drought stress (Martínez García et al. 2024). At the same time, the general tendency of both GPP and Re to increase with increasing VPD was preserved in the drought conditions (Fig. 6), likely for the reason of persistently high PAR, air and soil T at the times of atmospheric drought.

Soil and air droughts may either coincide, or occur separately. Most of the 2021 drought was manifested as VPD stress, with low soil water content occurring only in the second half of July (Fig. 3). Periods of air drought occurred in May and August 2020 and May 2021, when SPEI showed no meteorological drought, and soil water was kept up by regular precipitation. Whether soil drought imposed any additional stress on the Norway spruce trees in this study is unclear. The EC data showed enhanced photosynthesis on the combined soil and air drought days in the Harvest block in 2021, which had a sufficient number of drought days on the record.

While the drought thus suppressed the photosynthetic efficiency in 2021, as was reliably shown by the CO_2 exchange in Control, the mounting soil dryness and prolonged VPD stress do not seem to have had a similar effect in June-July 2021. Both P_{max} and GPP increased throughout the drought of 2021, as well as during the hotter period of 2020 (Figs. 4-6).

It is unlikely that the weather of pre-harvest year 2020 augmented the drought response of 2021. Mid-late summer drought was shown to influence the growth in the following year (Laurent 2003) via effects on bud formation (Salminen and Jalkanen, 2005), carbon allocation (Waring and Franklin, 1979), carbohydrate reserves for bud expansion and initial growth in the next growing season (Bouriaud and Popa 2009). However, the weather of July-September 2020 was mild in terms of air temperature and soil water content.

4.1.3 Thinning effects

Thinning intensity affects the drought sensitivity of a stand (Kohler et al. 2010, Misson et al. 2003). However, the previous studies generally agree on increased drought resistance and recovery as a result of partial harvest (Elkin et al. 2013, Manrique-Alba et al. 2020, Giuggiola et al. 2013, Sohn et al. 2016). This study found the majority of Control block trees to increase their transpiration during air drought (increasing evaporative demand), whereas an opposite dynamic was in place at Harvest (Fig. 7). This relative sap flow deficit at Control may be seen as a dip between 12-16 PM, when the VPD is at the maximum (Fig. 8). The shape of mean SF vs. VPD curve in summer-2021 was similar between the trees in both blocks, in contrast to the report of highly heterogeneous sap flow patterns during the extreme 2003 drought (Gartner et al. 2009). Additionally, the possible positive effect of thinning follows from the analysis of light response curves, as the post-selection harvesting (CCF) light response curve is higher at air & soil drought than at no drought condition, while the opposite holds in regard to pre-harvest conditions (Fig. 5c,d).

Thinning increases individual tree transpiration but decreases transpiration at stand level (e.g. Laurent et al. 2003), and in this study, the selection-harvested block showed a twice lower transpiration than the Control

https://doi.org/10.5194/egusphere-2026-568
Preprint. Discussion started: 5 February 2026

block, based on upscaled tree sap flow data of the 2021 growing season (Fig. 9). Thus, this study supports the previous observations that a thinned stand exhibits a drop in total transpiration, even if the individual trees are able to transpire more than they did before the thinning. For instance, removal of 61% of basal area led to mean tree-level sap flow increase of 27%, but a 34% reduction in the stand-level transpiration (Zavadilova et al. 2023).

The ratio between the upscaled SF and EC ET stayed constant during the drought of 2021, and its mean value of 0.7 was substantially higher than approx. 0.5 predicted for a similar stand with LAI = 2 m^2 m^{-2} by a process-based model (Leppä et al. 2020, Fig. 12). Such a dominance of tree transpiration over forest floor ET is common in mature forests, particularly in drought conditions (Launiainen et al. 2019, Martínez-García et al. 2024).

The decline in transpiration during drought is further reflected in Bowen ratio changes; the mean daytime June-July Harvest BR was 0.33 in 2020 and 1.49 in 2021, while the Control BR was respectively 0.25 in 2020 and 0.95 in 2021. McGloin et al. (2019) identified similar drought-induced increases in the Bowen ratio of two Czech Norway spruce stands, from 1.52 to 2.50 - 2.70. In the current study, CWSI gave qualitatively similar information to BR and temperature-based stomatal conductance.

4.2 Towards early detection of drought stress: potential and limitations of different monitoring tools

4.2.1 Sap flow and UAV remote sensing data

Assessing the spatial diversity in tree transpiration is essential for early detection of drought stress. This can be done by UAV-based remote sensing and by sap flow measurements. Therefore, the search for the trees that are the first to exhibit drought reaction was one of the aims of the present study. Our findings suggest that there were indeed a minority of trees which are not resilient to drought. In Harvest, these trees revealed themselves by increased canopy temperature and lowered NDVI, while in Control the stress was detectable based on constrained sap flow.

The relative transpiration deficit in the individual trees in the Control block was well detected by sap flow sensors (Sect. 3.3, Figs. 7,8). The afternoon sap flow deficit in the monitored Control block trees, in relation to those in the Harvest block, is a clear sign of water stress in the afternoon when the VPD is at its diurnal peak (Fig. 8). This is further illustrated on an individual tree basis by stagnating sap flow increase at high VPD under soil drought conditions.

However, UAV remote sensing indicated a considerable increase in the spatial heterogeneity of individual tree canopy temperature and NDVI, which may also be interpreted as increase in stress relative to the reference (non-drought) period (Sect. 3.4, Figs. 10). However, the inter-tree differences in temperature and NDVI at peak drought are higher in the Harvest than Control (Figs. 10-11), which conflicts with the direct evidence of higher drought stress in the Control block obtained from sap flow data. In particular, the trees in the first row the ditches in the Harvest block have markedly lower NDVI and generally warmer canopies than those further away from the ditches, but are not measured by sap flow sensors; they therefore are possibly stressed, but we cannot verify this for lack of direct monitoring data of these specific trees. The variation in the degree of mutual shadowing by the trees is an unlikely reason for this spatial trend, as the Harvest has a uniformly low tree density and the drone flights were conducted at the time of the highest solar elevation. A similar spatial picture

https://doi.org/10.5194/egusphere-2026-568
Preprint. Discussion started: 5 February 2026

can be seen along some major ditches in the Control block (Fig. 10). Hence, it is possible that the trees monitored with sap flow sensors in the Harvest block do not cover the range of drought stress response that occurs within the Harvest, and possibly likewise in the Control block. A further aspect that may have influenced the assessment of stressed trees in the pre-drought and drought NDVI maps is the fact the pre-drought NDVI data was obtained before noon, while the drought data were sampled in the afternoon, when maximum drought stress is shown by sap flow sensors.

Notwithstanding the uncertainties, more on which will be said below, UAV remote sensing has an undeniable strength in that it allows assessing the statistics of individual tree parameters within a stand. In the present study, the increase in the inter-tree disparity in NDVI (Fig. 10h), canopy temperature and the derived T-based stomatal resistance under drought, (Fig. 11b) may be considered to be an indication of stress in trees, as the least resilient trees show more extreme values of vegetation indices compared with the main tree population.

4.2.2 UAV data for drought detection: benefits and limitations

UAV mapping is a very useful tool enabling the study of spatial distributions of canopy and ground colour, reflectance, temperature and structure. However, the UAV data also have substantial limitations complicating the analysis of tree drought response that do not have immediate solutions. These concern both the multispectral data and thermal data. Canopy segmentation is a first important step that presented a greater challenge in the dense canopy of the Control block (Appendices A, C). The large number of trees that could not be segmented required a statistics-based correction (Appendix C). The dominant trees are more sensitive to climate and weather, being more exposed to wind, VPD stress and solar radiation (Schmied 2022). The UAV data users should therefore be aware of the biases associated with the UAV tree health proxies in stands with non-uniform tree spacing and age.

The separation of canopy and ground pixels in the UAV multispectral and thermal orthomosaics is an issue common for all sensors. In the present experiment, the Normalized Green-Red Difference Index NGRDI was used (Appendix C), and performed well based on visual examination. However, we acknowledge that the greenness threshold segregating spruce needles from ground varies across the survey area due to the differences in tree vs. ground colour, both between the individual trees, and between the Control and Harvest blocks. The relatively open canopies of the Norway spruce pose an additional challenge to segregate the shoots from the woody parts and the ground.

A further two considerations apply to thermal imaging. One is the small-scale variability in aerodynamic conductance in the vicinity of each tree, or, in other words, wind-induced cooling and enhancement of transpiration. The trees that are sheltered from the wind experience a lower VPD and less wind-induced leaf cooling than other trees that are more exposed (e.g. Zweifel et al. 2005). This has direct consequences for the estimation of stomatal conductance based on leaf temperature (Sect. 3.4, Fig. 10, Appendix D). Such tree-scale variations in the field of turbulence are difficult or impossible to measure directly, so that Large Eddy Simulation of wind flow through forest canopy becomes the only feasible tool to tackle this problem. Accounting for inter-tree differences in aerodynamic conductance and amount of received solar radiation will enable more precise interpretation of canopy temperature.

https://doi.org/10.5194/egusphere-2026-568
Preprint. Discussion started: 5 February 2026

The initial expectation was that the stressed trees would show both low Tree-mean NDVI and low temperature-derived stomatal conductance. A positive relationship is indeed observed in the Control, but the absence of correlation between the individual canopy NDVI and temperature-based stomatal conductance in the Harvest block that is observed in late July 2021 data is difficult to explain (Fig. 12). NDVI showed a positive correlation with tree height in Control, but the correlation was not detectable in Harvest, which could be partly due to the previously observed NDVI saturation over dense stands (Vicca et al. 2016).

4.2.3 EC CO_2 flux as ecosystem-average drought proxy

In contrast with the tree-specific information provided by sap flow sensor data, Eddy-Covariance drought stress proxies are known to be inherently area-averaging, and thus incapable of precisely detecting short-term changes in the physiology of a subset of trees within a stand. In the present study, the EC fluxes are mainly representative of the Harvest block (Appendix B), while the amount of data from Control is deemed too low to serve as reliable basis for drought stress estimation. This further diminishes the possibility of detecting the stress in the minority of non-resilient trees within Control which was identified by sap flow data. While the sequence of Norway spruce drought responses was found to be always the same (drop in stomatal conductance, photosynthesis, leaf potential, chlorophyll), the stress level controlled the timing and magnitude of responses (Ditmarova et al. 2010). The more resilient Norway spruce trees have water reserves to withstand several days of drought stress without showing pronounced reactions (Ditmarova et al. 2010, Čermák *et al.*, 2007). Consequently, trees within a stand would respond to drought with a widely varying lag, complicating the interpretation of EC data.

The upscaling of sap-flow to the Harvest and Control blocks and EC footprint demonstrated a close match between the two independent transpiration measurement techniques (Sect. 3.3, Fig. 9). While tree transpiration comprised a larger fraction of the total ET during the hot June-July period of 2021, this ratio was not altered by the initiation of soil drought in the late June 2021. In general, it seems that the 2021 drought was also not strong enough to affect the seasonality in tree growth (Appendix H, Fig. H1), carbon uptake (Fig. 4) and transpiration (Fig. 9), although it did induce relative deficits in all these parameters. From the tree viewpoint, the relative moderateness of the drought follows from the observation that sap flow and transpiration did not decouple from potential evapotranspiration (Fig. 9).

The difference in drought reaction timing between the individual trees in a stand is often ignored in studies based on eddy-covariance technique. While it is a useful tool providing continuous data on CO_2 and H_2O surface exchange, it yields fluxes averaged over a large area, typically a few ha to over 1 km^2 in size (Rebmann et al. 2018). Because of this averaging nature of the EC method, its users can only detect drought responses as substantial changes in ecosystem-average carbon, water and energy fluxes - when (and if) such changes occur. Even over reasonably homogeneous stands, any change in EC footprint might lead to significant differences in estimated NEE and its components, further highlighting the challenge of EC flux attribution to smaller elements of the landscape (Krasnova et al. 2022). Furthermore, the contributions of the ground and trees to the total 30 min exchange rates in EC data are difficult to estimate (Subke and Tenhunen, 2004; Aslan et al., 2024).

5 Conclusions

https://doi.org/10.5194/egusphere-2026-568
Preprint. Discussion started: 5 February 2026

The results of this study complement the existing knowledge on the ecophysiology of Norway spruce-dominated boreal forests exposed to episodic droughts. Boreal ecosystems typically show an increase in GPP during moderate droughts due to prevalence of sunny weather under drought, although the reduction in the CO_2 uptake caused by the tightened stomatal control, decline in photosynthetic capacity and higher respiration tend to curtail any enhancement in net CO_2 sink. These factors indeed reduced the NEE in Ränskälänkorpi in June-July 2021.

The Norway spruce trees were found to exhibit stomatal regulation as an immediate defensive measure against water loss, although the drought did not significantly constrain stem radial growth (Appendix H). However, the different ecosystem monitoring tools (eddy-covariance, sap-flow sensors and UAS-based remote sensing) gave rather different indications regarding the drought stress caused by the early stages of a drought.

It is proposed that early detection of drought stress in a stand is possible only via analysis of individual tree sap-flow data, while the applicability of eddy-covariance data is inferior due to being area-integrating, and the UAV remote sensing data have coarse temporal coverage. In order to improve the quality of now- and fore-casting of drought stress, it is further suggested that the sap-flow sensors be installed in trees representing the whole range of health and resilience within the stand, so that the most disadvantaged trees would act as indicators of drought onset.

Appendices

Appendix A. Projected canopy cover

Projected canopy cover was calculated as the total area of the tree canopies identified in orthomosaics from 15th September 2020 and 26 July 2021 to the total area of the Harvest and Control blocks. Canopy projected area was somewhat lower in the Harvest block in 2020 prior to selection harvest, about 60% compared with 75% in the Control block (Table A1). Post-selection harvest in 2021, the Harvest block canopy cover was down to 22%. The tree locations identified in the two UAV surveys are shown in Fig. A1(a,b). The tree canopy area distributions prior to selection harvest were nearly identical in the two blocks (Fig. A1c). The distribution for Control shows slightly larger canopies, which might be in part related to the higher challenge of separating the overlapping canopies in the parts of Control block where the tree density was higher. After the selection harvest, the tree area in the Harvest block became strongly reduced (Fig. A1c), indicating that large trees were primarily harvested; the increase in the number of small trees is due to the fact that detection of small trees was facilitated by the removal of large trees.

https://doi.org/10.5194/egusphere-2026-568
Preprint. Discussion started: 5 February 2026

Table A1. Total areas of the Harvest and Control blocks, the total projected canopy area, and the projected canopy cover fraction.

	15 Sep 2020	**26 July 2021**
Harvest block total area	47383 m^2	
Control block total area	56940 m^2	
Harvest tree projected area	28278 m^2	10573 m^2
Control tree projected area	35690 m^2	36530 m^2
projected canopy cover, Harvest block	59.8%	22.3%
projected canopy cover, Control block	75.3%	75.3%

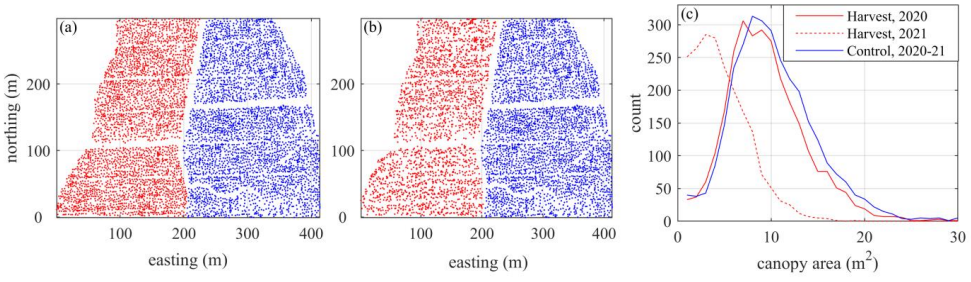

Figure A1. (a) tree locations in the Harvest (red) and Control (blue) blocks prior to selection harvest, based on the 15 September 2020 UAV survey; (b) same as (a), but for post-selection harvest, based on 26 July 2021 UAV survey; (c-d) tree canopy area distributions for Harvest and Control blocks before and after the selection harvest, respectively.

https://doi.org/10.5194/egusphere-2026-568
Preprint. Discussion started: 5 February 2026

Appendix B. Eddy-covariance footprint

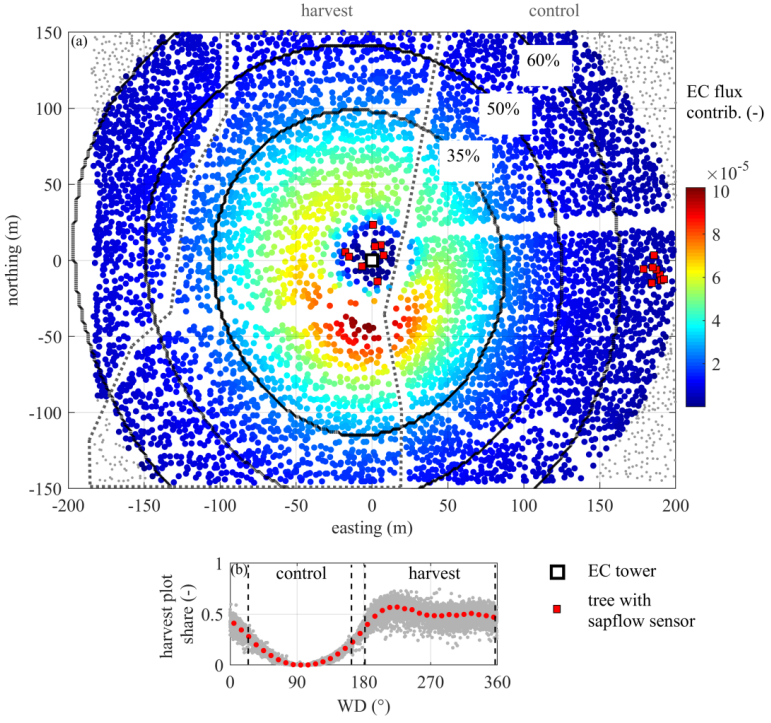

Figure B1. (a) Eddy-covariance footprint isolines (bold lines) and the individual tree contributions to cumulative source of the estimated turbulent fluxes (coloured dots). The colours of dots represent the cumulative summertime EC footprint. The EC tower is located in the center of the imaged area (the white square); northing and easting are calculated relative to the EC tower. The trees with sap flow sensors are shown with red squares. The Harvest block boundary is marked with a dotted line. (b) dependence of Harvest block contribution to the overall EC flux on wind direction; the rest is the Control block contribution. The grey dots are 30 min averages; the red dots are 10° bin-averages.

As follows from Fig. B1a, the peak portion of the footprint falls at about 100 m distance from the EC tower. The cumulative footprint is approximately circular. The trees contributing the most to the estimated turbulent fluxes are therefore located at distances of ca. 25-100 m from the tower, in the SE-S-W sector. the Harvest block contributes at most 50-60% to the total EC signal source, at S-SW winds (Fig. B1b); the rest of the source is contributed by the Control block or extends beyond the research area. The maximum contribution of the Control block approaches 100% in the eastern sector.

https://doi.org/10.5194/egusphere-2026-568
Preprint. Discussion started: 5 February 2026

Appendix C. Processing of UAV imagery and tree canopy segmentation

A rubber pool filled with water was used as an absolute temperature reference. The pool water temperature was recorded every 10 s by a logger with two T sensors immersed in shadow locations on the opposite ends of the pool (see Appendix D for the setup photo). The water was continuously mixed by a portable pump to ensure that the sensor readings corresponded to surface water temperature. The pool temperature was calculated as the average of the readings of the two T sensors for the duration of the UAV flight. The absolute T of the thermal orthomosaics was thus corrected for the mean temperature offset by subtracting from all pixels the difference between the real T of the water pool and the T extracted from the thermal orthomosaic (Table 1). The original post-processed, corrected orthomosaics of surface temperature and NDVI before canopy segmentation are presented in Appendix E.

Tree canopy segmentation is based on an algorithm developed by Silva et al. (2016), which delineates the crowns using centroidal Voronoi tessellation based on tree tops detected using local maxima filtering (Popescu et al., 2004) individual tree detection (ITD). As the trees in the site are generally have a small width compared with height, a narrow search window less than 2 meters was required in order to find the local maxima (tree tops) from the Canopy Height Model (CHM). However, such a small window generates artificial tops in non-apex points of trees such as in upward-bending branches. Those tops were removed by examining the neighborhood of each top in the CHM by removing the false tops near ground pixels as the true tree top is expected to be located near the center of the crown ground projection.

Since the trees remaining in the harvest site are narrow and have tops detected near the edges of the crowns, the top neighborhood in CHM did not yield enough information to label the top as incorrect. As there were two flights made in the same area a year apart, the tops could be clustered by distance to correspond to a top detected in the previous survey which had fewer incorrect tops, and only a single top for each tree was assigned. With these two methods, almost all incorrect tops are removed in the Control block. In selection Harvest block, only about 5% of the remaining tops are incorrect, which is we consider as good method performance for such a dense natural canopy. The methods also successfully remove the incorrect tops detected in CHM noise points, which are caused from lower image overlap in certain areas in 2021 RGB survey.

In 2020, individual tree detection was carried out in an area of 20 hectares, yielding 10188 trees in total; of these, 9202 trees had $h > 15$ m. In 2021, the area was 12 hectares, yielding 6612 trees with $h > 0$, including 5820 trees with $h > 15$ m.

For individual tree level analysis, the trees in 2020 and 2021 datasets are associated by finding the crowns with the highest overlap in area. In addition, the height difference is ensured to be less than 1 m so that correct trees are associated between the 2020 and 2021 data despite the larger number of smaller trees that are identified in the harvest plot thanks to the more open canopy after the selection harvest. In this way the slight georeferencing difference between the orthomosaics could be ignored and each associated 2020-2021 tree pair was given a unique ID.

Next, the individual tree canopy bands were calculated as the means of the orthomosaic pixels lying inside the tree canopy boundaries. The non-foliage ground pixels in the canopy segments were removed by choosing a NGRDI threshold value that was found to most efficiently separate the tree foliage from the woody tree parts and the ground. The canopy mean RGB brightness was also calculated as the mean value of the RGB camera

https://doi.org/10.5194/egusphere-2026-568
Preprint. Discussion started: 5 February 2026

bands (Fig. 10e,f). The mean calibrated R and NIR band values from the multispectral camera orthomosaic were used to calculate the tree-mean NDVI index values (Fig. 10g,h). The canopy-mean temperatures were obtained from the surface temperature map, and subsequently corrected for the brightness variations among the canopies, in order to eliminate the effect of unequal incident radiation (Appendix G). For each crown, a range of features such as canopy mean temperature (T_c) NDVI, RGBVI and NGRDI vegetation indices were calculated from the pixels lying within the segmented canopy. Finally, the temperature-based stomatal conductance was calculated using Eq. (9) (Fig. 10a,b).

As the UAV images show only the top of the canopy layer, the ITD process for the 2021 imagery detects approximately 50% of the trees in the control areas and 80% in the selection harvest area when compared to Terrestrial Laser Scanning (TLS) campaigns undertaken in two 50x50m survey areas in the control and harvest plots in spring 2021 after the selection harvest. To correct this bias, the true size distribution of all trees in the site was modeled using a Horvitz-Thompson-type approach developed by Kansanen et al. (2022), which estimates the detectability (α) of each tree. Here, the trees are ordered by height, and the tallest tree are assigned the detectability equal to 1. For the rest of the trees, the number of trees could be calculated using α. This method corrects the distribution for the set of trees with height detected using ITD, but does not sufficiently correct the bias for trees with height less than 10 meters since these remain mostly unseen in the UAV photos. The trees with heights of less than 5 meters are also mostly undetected in the TLS surveys. α may also be understood as an estimate of the overall success of the UAV imaging and the methodology used to identify and segment the canopies form the UAV data.

Appendix D. References for thermal and multispectral measurement

Estimation of individual tree stomatal conductance from UAV-measured crown temperature involved a set of references presented in Fig. D1. The two branch piles, wet and dry, represent the freely evaporating and non-evaporating canopies, respectively. Both branch piles are placed on a frame elevated ca. 70 cm from the ground in order to allow aeration from the bottom, in order to closer imitate the aerodynamic conductance profile of a real tree canopy. The wet branch pile is amply sprayed with water by means of a watering bucket, resulting in a temperature contrast as shown in the right-hand part of the figure. Nearby, a water pool for absolute temperature correction was set up, with a small pump continuously mixing the water, and two temperature sensors suspended near the surface in the opposite ends of the pool.

The multispectral reference was a 1 m^2 steel sheet painted gray, placed near the thermal references.

https://doi.org/10.5194/egusphere-2026-568
Preprint. Discussion started: 5 February 2026

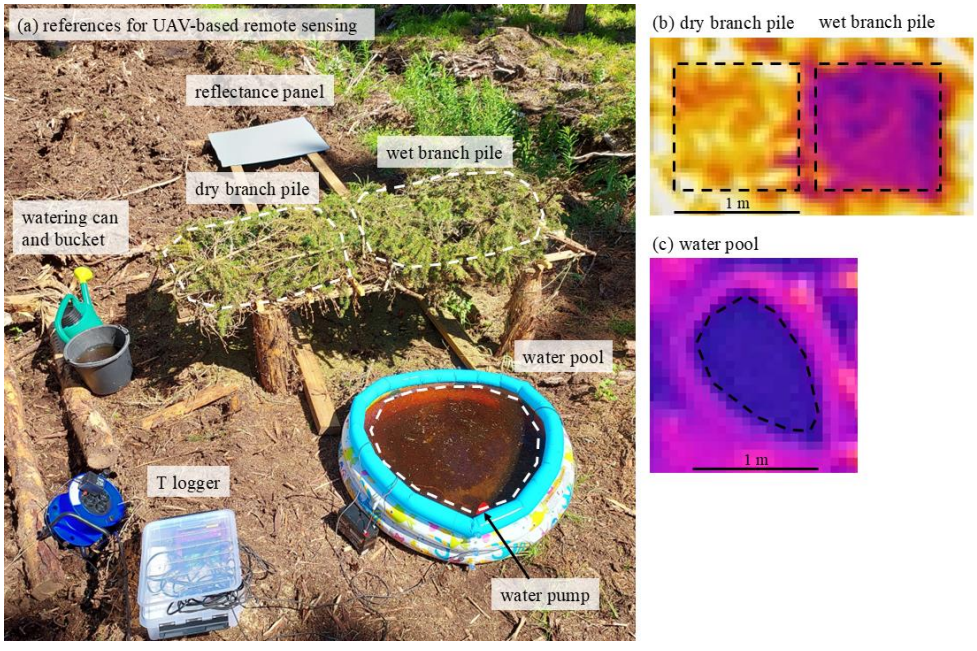

Figure D1. Ground references for stomatal resistance estimation after adapted to the forest case. A ground photo and the views of the references as registered by the thermal camera from a 40 m altitude a.g.l.

Appendix E. Monitored tree parameters and sap-flow upscaling

Sap flow data were measured in 7 trees in the control and 8 trees in the harvest sites. The sap flow time series were quality controlled by visual inspection and apparently faulty periods removed based on high random error, scatter or unrealistic daily sap flow pattern. The periods that were offset to the positive nighttime values but retained a realistic diurnal pattern were corrected, separately for each day, by adjusting the sap flow values with a constant value added to each day so that the mean of the sap flow values between 0 and 4 AM becomes zero. The parameters of the sap flow trees are summarized in Table E1.

https://doi.org/10.5194/egusphere-2026-568
Preprint. Discussion started: 5 February 2026

Table E1. Parameters of the spruce trees monitored with sap flow and stem diameter sensors.

plot	Tree ID	height (m)	DBH (mm)	age (years)	sapwood depth (mm)	density (kg m^{-3})	sapwood area (m^2)
Control	1	22.2	282	78	40	363	0.030
	2	21.5	295	75	33	370	0.027
	3	20.9	234	76	44	383	0.026
	4	18.9	200	92	51	387	0.024
	5[#]	12.6	116	55	28	424	0.008
	6	15.4	160	74	19	423	0.008
	7	14.4	128	43	18	417	0.006
	8	13.6	116	58	26	432	0.007
Harvest	9	19.7	200	76	53	395	0.018
	10	23.3	254	87	44	359	0.029
	11	21.3	273	93	39	342	0.029
	12	19.2	210	51	44	362	0.023
	13	15.9	136	53	29	404	0.001
	14	10.9	94	47	15	428	0.004
	15	18.8*	177	60	40	396	0.017
	16	12.2	107	49	27	428	0.007

[#] Tree No. 5 was not used due to the technical issues with the sap flow sensor.

* The height is estimated using the DBH-height relationship derived for this site (not shown). The tree No. 5 is excluded from sap flow analyses due to the issues with its sap flow sensor, but is retained in dendrometer analyses.

The fitting of a power function $y = ax^b$ where y is the sap flow, x the tree height, and a,b the fit coefficients was done separately to the harvest and control trees. See Fig. E1 for an example of an upscaling curve. As sap flow was not measured in trees under 10 meters in height, an assumption is made that the trees with infinitesimally small height have zero sap flow, in order to anchor the fit to the point of origin. This fitting procedure might lead to certain overestimation of sap flow in trees with heights of under 10 m, as the smaller trees are typically shaded more than the taller trees, which limits their sap flow. Nevertheless, this is of minor importance for the total upscaled sap flow of the forest, as the stand-scale sapflow is mainly contributed by large trees. Sap flow of each individual tree detected in drone orthomosaics is calculated from the regressions for the Control and Harvest blocks.

The radial growth of the trees detailed in Table E1 is presented in Appendix H.

https://doi.org/10.5194/egusphere-2026-568
Preprint. Discussion started: 5 February 2026

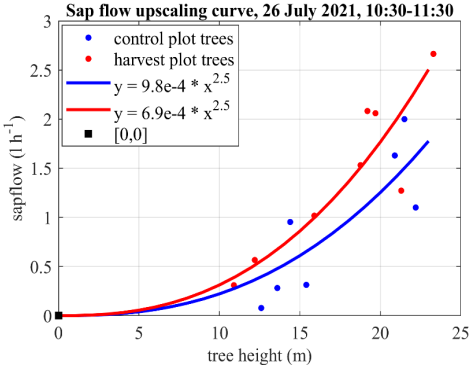

Figure E1. An example of sap flow *vs.* tree height curves used for upscaling from tree to forest scales, averaged for the duration of the 4th UAV flight on 26 July 2021.

For the harvest and control plots, the total sap flow is a simple sum of sap flows modeled for each tree. The total sap flow within the EC flux source area was achieved by weighing the individual tree sap flow values by the individual tree EC footprint values. In order to facilitate the comparison of the upscaled sap flow with ET derived from the EC latent heat flux, the upscaled sap flow values were expressed in the units of mm d^{-1}.

https://doi.org/10.5194/egusphere-2026-568
Preprint. Discussion started: 5 February 2026

Appendix F. Original UAV maps of surface T and NDVI

The original surface temperature and NDVI orthomosaics obtained in 2020 and 2021 are presented in Fig. F1.

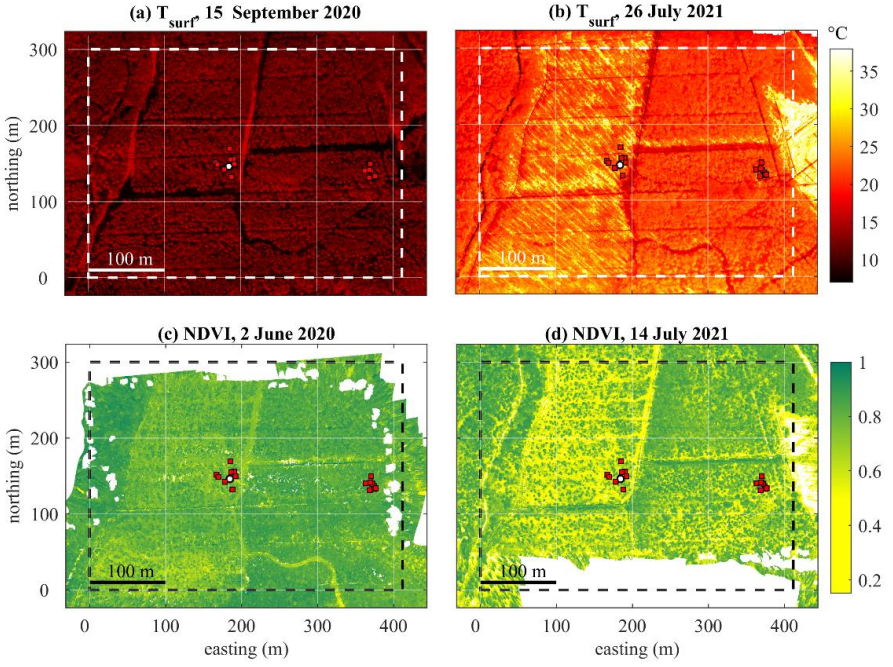

Figure F1. (a,b) the original thermal orthomosaics based on the UAV flights on the 15th September 2020 and 26 July 2021, before canopy segmentation. (c,d). The original NDVI orthomosaics of 2 June 2021 and 14 July 2021. The mapped area and legend are as in Fig. 1.

https://doi.org/10.5194/egusphere-2026-568
Preprint. Discussion started: 5 February 2026

Appendix G. Brightness correction of canopy temperature

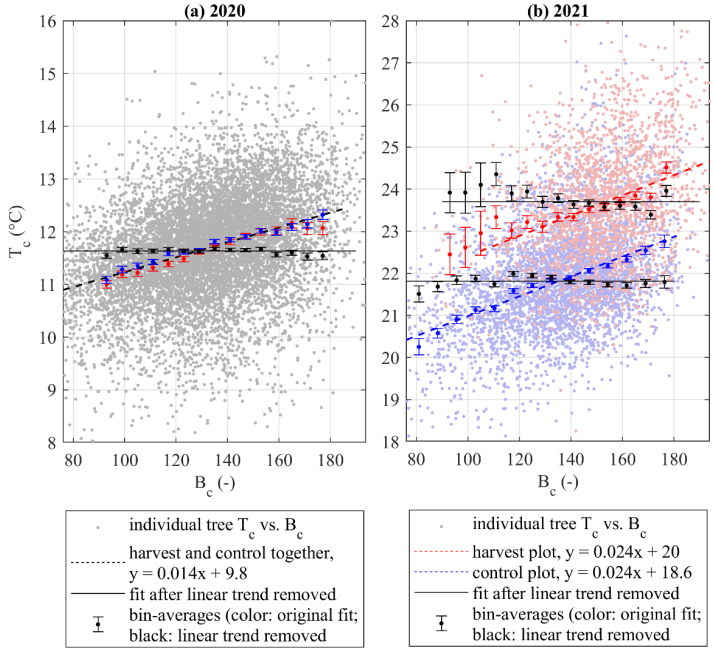

Figure G1. Canopy temperature versus canopy brightness for the UAV flight data of 15 Sep 2020 (a) and 26 July 2021 (b).

Contrasting relationships between canopy brightness and temperature were observed in the data of 15 Sep 2020 (pre-harvest) and 26 July 2021 (after harvest, during drought) (Fig. G1). The regression lines of control and harvest practically coincide on 15 Sep 2020 and differ mainly by the intercept on 26 July 2021 (18.7 and 20.0 ˚C, respectively), the slope being almost equal (0.024). The main difference between the two flights is found in the slope of the T_c vs B_c regression between the two dates, 0.014 and 0.024, respectively. Based on this evidence of a pronounced effect of canopy brightness on canopy temperature, the corrected canopy temperature (with the brightness effect eliminated) was calculated by subtracting from T_c the linear relationship between T_c and B_c. Then, the corrected version of the temperature-based stomatal resistance $r_{sT,corr}$ was calculated (Eq. 11) using the brightness-corrected T_c.

https://doi.org/10.5194/egusphere-2026-568
Preprint. Discussion started: 5 February 2026

Appendix H. Stem radial growth

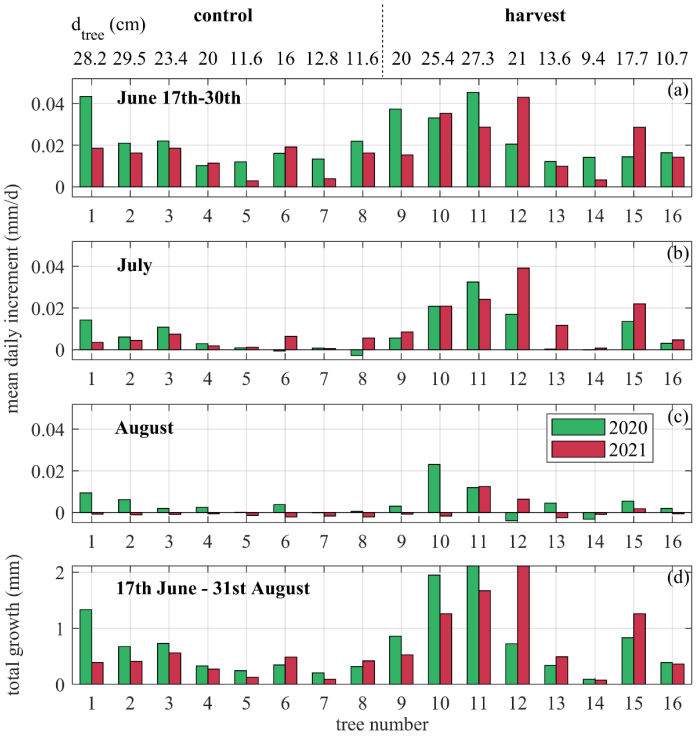

Figure H1. Tree diameter increment for the monitored trees in Control and Harvest blocks in 2020 and 2021. Mean daily stem diameter increment in (a) 17th-30th June, (b) July and (c) August; (d) total growth in 17 June – 31 August.

17-30th June is used as the period of good dendrometer data coverage in 2020, and used also for 2021 for the sake of consistency. 2020 and 2021 display the normal seasonality of Norway spruce stem diameter in southern Finland, with some differences between Control and Harvest (Fig. H1). The trees monitored with dendrometers show generally more growth in the Harvest block than in the Control block, in all months and in over the whole summer. The only exception in the Control is the dominant tree No. 1 that in 2020 showed growth comparable with the fastest growing trees in the Harvest block. The growth in June was the greatest of all summer months in both blocks and both years; it slowed down considerably in July and August, particularly in Control. In August 2021, most trees showed small stem shrinkage, except for trees No. 11, 12 and 15 (all in Harvest), which did grow slightly.

https://doi.org/10.5194/egusphere-2026-568
Preprint. Discussion started: 5 February 2026

Code and data availability

The complete dataset and codes used in this work are available on request from the leading author.

Acknowledgements

We are grateful to Prof. Lauri Mehtätalo (Natural resources Institute Finland) who provided advice on the statistical corrections to the tree population derived from the UAV maps and the sap flow upscaling approach. The team of engineers responsible for the measurements at the Ränskälänkorpi site are gratefully acknowledged.

Financial support

We acknowledge the financial support of ICOS Finland by University of Helsinki. PA gratefully acknowledges the Postdoctoral grant from the Research Council of Finland for the project DRONESTRESS (decision no. 351129). PA and SL acknowledge the support from the EU Horizon 2020 Framework Programme, EU H2020 Excellent Science (GreedFeedBack, grant no. 101056921) and the Research Council of Finland (grant no. 356138). MM acknowledges funding from the Postdoctoral Programme for Research Institutes in Finland. EL acknowledges funding the Interreg Northern Periphery and Arctic Programme, Co-funded by the European Union, project FORESTCARBOVISION (NPA0800248); funding from Research Council of Finland, the Academy of Finland Flagship Programme (Forest-Human-Machine Interplay (UNITE)) grant no. 337653; funding from Business Finland, project Digital Forest Carbon Twins. We are grateful for the Research Council of Finland Flagship Programme for financial support (UNITE Flagship, 359174). This project has received funding from the Research Council of Finland (grant no. 374131, 372822). We are also grateful for the support of the ACCC Flagship funded by the Research Council of Finland (grant no. 337552).

Author contributions

PA formulated the study framework, conducted UAV flights, analyzed the data and prepared the manuscript. MP helped formulate the conceptual framework, contributed to the manuscript, provided commentary on tree physiology, conducted in-situ tree measurements and provided the relevant field data. RM provided general supervision, made contributions on CCF- and stand structure-related topics, and wrote parts of the manuscript. VT processed and analyzed the UAV data, performed the statistical corrections of tree population data and contributed to the text. TL took care of eddy-covariance and meteorological data and contributed to the text. HJ provided expertise in thermal and multispectral remote sensing and helped interpret the relevant data. MM processed the UAV data, conducted the LAI and stand structure surveys, and wrote parts of the text. EL conducted UAV flights and processed the UAV data. HR contributed to the text and provided expertise on eddy-covariance data. TV provided the UAV equipment and contributed to the manuscript. SL provided overall supervision, helped conceptual framework, advised on the writing and data analysis, and wrote parts of the manuscript.

Competing interests

None of the authors has any competing interests.

https://doi.org/10.5194/egusphere-2026-568
Preprint. Discussion started: 5 February 2026

References

Aldea, J., Bianchi, S., Nilsson, U., Hynynen, J., Lee, D., Holmström, E., and Huuskonen, S.: Evaluation of growth models for mixed forests used in Swedish and Finnish decision support systems, For. Ecol. Manag., 529, 120721, https://doi.org/10.1016/j.foreco.2022.120721, 2023.

Alderfasi, A. A. and Nielsen, D. C.: Use of crop water stress index for monitoring water status and scheduling irrigation in wheat, Agric. Water Manag., 47, 69–75, 2001.

Alekseychik, P., Korrensalo, A., Mammarella, I., Launiainen, S., Tuittila, E.-S., Korpela, I., and Vesala, T.: Carbon balance of a Finnish bog: temporal variability and limiting factors based on 6 years of eddy-covariance data, Biogeosciences, 18, 4681–4704, https://doi.org/10.5194/bg-18-4681-2021, 2021.

Arend, M., Link, R. M., Patthey, R., Hoch, G., Schuldt, B., and Kahmen, A.: Rapid hydraulic collapse as cause of drought-induced mortality in conifers, Proc. Natl. Acad. Sci. USA, 118, e2025251118, 2021.

Aslan, T., Launiainen, S., Kolari, P., Peltola, O., Aalto, J., Bäck, J., Vesala, T., and Mammarella, I.: Thinning turned boreal forest to a temporary carbon source – short-term effects of partial harvest on carbon dioxide and water vapor fluxes, Agric. For. Meteorol., 353, 110061, 2024.

Aubinet, M., Vesala, T., and Papale, D. (Eds.): Eddy covariance: a practical guide to measurement and data analysis, Springer, 2012.

Balting, D. F., AghaKouchak, A., Lohmann, G., and Ionita, M.: Northern Hemisphere drought risk in a warming climate, npj Clim. Atmos. Sci., 4, 61, 2021.

Beniston, M. and Stephenson, D. B.: Extreme climatic events and their evolution under changing climatic conditions, Global Planet. Change, 44, 1–9, 2004.

Bennett, A. C., Penman, T. D., Arndt, S. K., Roxburgh, S. H., and Bennett, L. T.: Climate more important than soils for predicting forest biomass at the continental scale, Ecography, 43, 1692–1705, 2020.

Barbedo, J. G. A.: A review on the use of unmanned aerial vehicles and imaging sensors for monitoring and assessing plant stresses, Drones, 3, 40, 2019.

Berni, J. A. J., Zarco-Tejada, P. J., Suárez, L., González-Dugo, V., and Fereres, E.: Remote sensing of vegetation from UAV platforms using lightweight multispectral and thermal imaging sensors, Int. Arch. Photogramm. Remote Sens. Spatial Inf. Sci., 38, 6, 2009.

Bouriaud, O. and Popa, I.: Comparative dendroclimatic study of Scots pine, Norway spruce, and silver fir in the Vrancea Range, Eastern Carpathian Mountains, Trees, 23, 95–106, 2009.

Brunner, A., Valkonen, S., Goude, M., Hanssen, K. H., and Erefur, C.: Chapter 2: Definitions and terminology: What is continuous cover forestry in Fennoscandia?, in: Continuous Cover Forestry in Boreal Nordic Countries, edited by: Rautio, P., Routa, J., Huuskonen, S., Holmström, E., Cedergren, J., and Kuehne, C., Springer, Cham, 11–43, 2024.

Bréda, N., Huc, R., Granier, A., and Dreyer, E.: Temperate forest trees and stands under severe drought: a review of ecophysiological responses, adaptation processes and long-term consequences, Ann. For. Sci., 63, 625–644, 2006.

Danneyrolles, V., Boucher, Y., Fournier, R., and Valeria, O.: Positive effects of projected climate change on post-disturbance forest regrowth rates in northeastern North American boreal forests, Environ. Res. Lett., 18, 024041, 2023.

https://doi.org/10.5194/egusphere-2026-568
Preprint. Discussion started: 5 February 2026

Del Río, M., Pretzsch, H., Ruíz-Peinado, R., Ampoorter, E., Annighöfer, P., Barbeito, I., Bielak, K., Brazaitis, G., Coll, L., Drössler, L., and Fabrika, M.: Species interactions increase the temporal stability of community productivity in Pinus sylvestris–Fagus sylvatica mixtures across Europe, J. Ecol., 105, 1032–1043, 2017.

Ditmarová, Ľ., Kurjak, D., Palmroth, S., Kmeť, J., and Střelcová, K.: Physiological responses of Norway spruce (Picea abies) seedlings to drought stress, Tree Physiol., 30, 205–213, 2010.

D'Orangeville, L., Maxwell, J., Kneeshaw, D., Pederson, N., Duchesne, L., Logan, T., et al.: Drought timing and local climate determine the sensitivity of eastern temperate forests to drought, Glob. Change Biol., 24, 2339–2351, https://doi.org/10.1111/gcb.14096, 2018.

Dreyer, I., Antunes, S., Hoshi, T., Müller-Röber, B., Palme, K., Pongs, O., Reintanz, B., and Hedrich, R.: Plant K+ channel alpha-subunits assemble indiscriminately, Biophys. J., 72, 2143–2150, 1997.

Ecke, S., Dempewolf, J., Frey, J., Schwaller, A., Endres, E., Klemmt, H. J., Tiede, D., and Seifert, T.: UAV-based forest health monitoring: A systematic review, Remote Sens., 14, 3205, 2022.

Elkin, C., Giuggiola, A., Rigling, A., and Bugmann, H.: Short- and long-term efficacy of forest thinning to mitigate drought impacts in mountain forests in the European Alps, Ecol. Appl., 25, 1083–1098, 2015.

Erdem, Y., Arin, L., Erdem, T., Polat, S., Deveci, M., Okursoy, H., and Gültaş, H. T.: Crop water stress index for assessing irrigation scheduling of drip irrigated broccoli (Brassica oleracea L. var. italica), Agric. Water Manag., 98, 148–156, 2010.

Escos, J., Alados, C. L., Pugnaire, F. I., Puigdefábregas, J., and Emlen, J.: Stress resistance strategy in an arid land shrub: interactions between developmental instability and fractal dimension, J. Arid Environ., 45, 325–336, 2000.

Felsche, E., Böhnisch, A., Poschlod, B., and Ludwig, R.: European hot and dry summers are projected to become more frequent and expand northwards, Commun. Earth Environ., 5, 410, 2024.

Friedrichs, D. A., Trouet, V., Büntgen, U., Frank, D. C., Esper, J., Neuwirth, B., and Löffler, J.: Species-specific climate sensitivity of tree growth in Central-West Germany, Trees, 23, 729–739, 2009.

Galiano, L., Timofeeva, G., Saurer, M., Siegwolf, R., Martínez-Vilalta, J., Hommel, R., and Gessler, A.: The fate of recently fixed carbon after drought release: towards unravelling C storage regulation in Tilia platyphyllos and Pinus sylvestris, Plant Cell Environ., 40, 1711–1724, 2017.

Gartner, K., Nadezhdina, N., Englisch, M., Čermak, J., and Leitgeb, E.: Sap flow of birch and Norway spruce during the European heat and drought in summer 2003, For. Ecol. Manag., 258, 590–599, 2009.

Gebhardt, T., Häberle, K.-H., Matyssek, R., Schulz, C., and Ammer, C.: The more, the better? Water relations of Norway spruce stands after progressive thinning, Agric. For. Meteorol., 197, 235–243, 2014.

Giuggiola, A., Bugmann, H., Zingg, A., Dobbertin, M., and Rigling, A.: Reduction of stand density increases drought resistance in xeric Scots pine forests, For. Ecol. Manag., 310, 827–835, 2013.

Gonzalez-Dugo, V., Zarco-Tejada, P., Berni, J. A., Suarez, L., Goldhamer, D., and Fereres, E.: Almond tree canopy temperature reveals intra-crown variability that is water stress-dependent, Agric. For. Meteorol., 154, 156–165, 2012.

Guilioni, L., Jones, H. G., Leinonen, I., and Lhomme, J.-P.: On the relationships between stomatal resistance and leaf temperatures in thermography, Agric. For. Meteorol., 148, 1908–1912, 2008.

https://doi.org/10.5194/egusphere-2026-568
Preprint. Discussion started: 5 February 2026

Gómez-Candón, D., Virlet, N., Labbé, S., Jolivot, A., and Regnard, J.-L.: Field phenotyping of water stress at tree scale by UAV-sensed imagery: new insights for thermal acquisition and calibration, Precis. Agric., 17, 786–800, 2016.

Hammond, W. M., Williams, A. P., Abatzoglou, J. T., et al.: Global field observations of tree die-off reveal hotter-drought fingerprint for Earth's forests, Nat. Commun., 13, 1761, 2022.

Härkönen, S., Lehtonen, A., Manninen, T., Tuominen, S., and Peltoniemi, M.: Estimating forest leaf area index using satellite images: comparison of k-NN based Landsat-NFI LAI with MODIS-RSR based LAI product for Finland, Boreal Environ. Res., 20, 181–195, 2015.

Hartmann, H., Ziegler, W., Kolle, O., and Trumbore, S.: Thirst beats hunger – declining hydration during drought prevents carbon starvation in Norway spruce saplings, New Phytol., 200, 340–349, 2013.

Hyyppä, E., Yu, X., Kaartinen, H., Hakala, T., Kukko, A., Vastaranta, M., and Hyyppä, J.: Comparison of backpack, handheld, under-canopy UAV, and above-canopy UAV laser scanning for field reference data collection in boreal forests, Remote Sens., 12, 3327, 2020.

Högberg, P., Ceder, L. A., Astrup, R., Binkley, D., Dalsgaard, L., Egnell, G., Filipchuk, A., Genet, H., Ilintsev, A., Kurz, W. A., and Laganière, J.: Sustainable boreal forest management challenges and opportunities for climate change mitigation, 2021.

Jackson, R. D., Idso, S. B., Reginato, R. J., and Pinter Jr., P. J.: Canopy temperature as a crop water stress indicator, Water Resour. Res., 17, 1133–1138, 1981.

Jactel, H., Petit, J., Desprez-Loustau, M.-L., Delzon, S., Piou, D., Battisti, A., and Koricheva, J.: Drought effects on damage by forest insects and pathogens: a meta-analysis, Glob. Change Biol., 18, 267–276, 2012.

Jia, X., Zha, T. S., Gong, J. N., Wu, B., Zhang, Y. Q., Qin, S. G., Chen, G. P., Feng, W., Kellomäki, S., and Peltola, H.: Energy partitioning over a semi-arid shrubland in northern China, Hydrol. Process., 30, 972–985, 2016.

Jones, H. G.: Plants and Microclimate, 2nd edn., Cambridge University Press, Cambridge, 1992.

Junttila, S., Vastaranta, M., Hämäläinen, J., Latva-Käyrä, P., Holopainen, M., Hernández Clemente, R., Hyyppä, H., and Navarro-Cerrillo, R. M.: Effect of forest structure and health on the relative surface temperature captured by airborne thermal imagery – case study in Norway spruce-dominated stands in southern Finland, Scand. J. For. Res., 32, 154–165, 2017.

Jönsson, A. M., Eklundh, L., Hellström, M., Bärring, L., and Jönsson, P.: Annual changes in MODIS vegetation indices of Swedish coniferous forests in relation to snow dynamics and tree phenology, Remote Sens. Environ., 114, 2719–2730, 2010.

Kansanen, K., Packalen, P., Lähivaara, T., Seppänen, A., Vauhkonen, J., Maltamo, M., and Mehtätalo, L.: Refining and evaluating a Horvitz–Thompson-like stand density estimator in individual tree detection based on airborne laser scanning, Can. J. For. Res., 52, 527–538, 2022.

Karkauskaite, P., Tagesson, T., and Fensholt, R.: Evaluation of the plant phenology index (PPI), NDVI and EVI for start-of-season trend analysis of the Northern Hemisphere boreal zone, Remote Sens., 9, 485, 2017.

Kimmins, J. P.: Forest Ecology, Macmillan Publishing Company, New York, 1987.

Kljun, N., Calanca, P., Rotach, M. W., and Schmid, H. P.: A simple two-dimensional parameterisation for Flux Footprint Prediction (FFP), Geosci. Model Dev., 8, 3695–3713, 2015.

https://doi.org/10.5194/egusphere-2026-568
Preprint. Discussion started: 5 February 2026

Kohler, M., Sohn, J., Nägele, G., and Bauhus, J.: Can drought tolerance of Norway spruce (Picea abies (L.) Karst.) be increased through thinning?, Eur. J. For. Res., 129, 1109–1118, 2010.

Kolb, T. E., Fettig, C. J., Ayres, M. P., Bentz, B. J., Hicke, J. A., Mathiasen, R., Stewart, J. E., and Weed, A. S.: Observed and anticipated impacts of drought on forest insects and diseases in the United States, For. Ecol. Manag., 380, 321–334, 2016.

Kopačková-Strnadová, V., Koucká, L., Jelének, J., Lhotáková, Z., and Oulehle, F.: Canopy top, height and photosynthetic pigment estimation using parrot sequoia multispectral imagery and the unmanned aerial vehicle (UAV), Remote Sens., 13, 705, 2021.

Kowalska, N., Šigut, L., Stojanović, M., Fischer, M., Kyselova, I., and Pavelka, M.: Analysis of floodplain forest sensitivity to drought, Philos. Trans. R. Soc. B, 375, 20190518, 2020.

Krasnova, A., Krasnov, D., Cordey, H. P. E., and Noe, S. M.: Eddy-covariance carbon fluxes of a heterogeneous forest: one tower-two heights, EGUsphere, 2022, 1–34, 2022.

Kuželka, K., Slavík, M., and Surový, P.: Very high density point clouds from UAV laser scanning for automatic tree stem detection and direct diameter measurement, Remote Sens., 12, 1236, 2020.

Launiainen, S., Guan, M., Salmivaara, A., and Kieloaho, A.-J.: Modeling boreal forest evapotranspiration and water balance at stand and catchment scales: a spatial approach, Hydrol. Earth Syst. Sci., 23, 3457–3480, https://doi.org/10.5194/hess-23-3457-2019, 2019.

Launiainen, S., Katul, G. G., Leppä, K., Kolari, P., Aslan, T., Grönholm, T., Korhonen, L., Mammarella, I., and Vesala, T.: Does growing atmospheric CO2 explain increasing carbon sink in a boreal coniferous forest?, Glob. Change Biol., 28, 2910–2929, 2022.

Laurent, M., Antoine, N., and Joël, G.: Effects of different thinning intensities on drought response in Norway spruce (Picea abies (L.) Karst.), For. Ecol. Manag., 183, 47–60, 2003.

Laurila, T., Aurela, M., Hatakka, J., Hotanen, J.-P., Jauhiainen, J., Korkiakoski, M., Korpela, L., Koskinen, M., Laiho, R., Lehtonen, A., Leppä, K., Linkosalmi, M., Lohila, A., Minkkinen, K., Mäkelä, T., Mäkiranta, P., Nieminen, M., Ojanen, P., Peltoniemi, M., Penttilä, T., Rainne, J., Rautakoski, H., Saarinen, M., Salovaara, P., Sarkkola, S., and Mäkipää, R.: Set-up and instrumentation of the greenhouse gas measurements on experimental sites of continuous cover forestry, Natural Resources and Bioeconomy Studies, 26/2021, Natural Resources Institute Finland, Helsinki, 51 pp., 2021.

Lasslop, G., Reichstein, M., Papale, D., Richardson, A. D., Arneth, A., Barr, A., Stoy, P., and Wohlfahrt, G.: Separation of net ecosystem exchange into assimilation and respiration using a light response curve approach: critical issues and global evaluation, Glob. Change Biol., 16, 187–208, 2010.

Leinonen, I., Grant, O. M., Tagliavia, C. P. P., Chaves, M. M., and Jones, H. G.: Estimating stomatal conductance with thermal imagery, Plant Cell Environ., 29, 1508–1518, 2006.

Leppä, K., Korkiakoski, M., Nieminen, M., Laiho, R., Hotanen, J.-P., Kieloaho, A. J., Korpela, L., Laurila, T., Lohila, A., Minkkinen, K., and Mäkipää, R.: Vegetation controls of water and energy balance of a drained peatland forest: responses to alternative harvesting practices, Agric. For. Meteorol., 295, 108198, 2020.

Lindroth, A., Holst, J., Linderson, M. L., Aurela, M., Biermann, T., Heliasz, M., Chi, J., Ibrom, A., Kolari, P., Klemedtsson, L., and Krasnova, A.: Effects of drought and meteorological forcing on carbon and water fluxes in Nordic forests during the dry summer of 2018, Philos. Trans. R. Soc. B, 375, 20190516, 2020.

https://doi.org/10.5194/egusphere-2026-568
Preprint. Discussion started: 5 February 2026

Liu, C., Peltoniemi, M., Alekseychik, P., Mäkelä, A., and Hölttä, T.: A coupled model of hydraulic ecophysiology and cambial growth—accounting for biophysical limitations and phenology improves stem diameter prediction at high temporal resolution, Plant Cell Environ., 48, 1344–1365, 2025.

Ludovisi, R., Tauro, F., Salvati, R., Khoury, S., Mugnozza Scarascia, G., and Harfouche, A.: UAV-based thermal imaging for high-throughput field phenotyping of black poplar response to drought, Front. Plant Sci., 8, 1681, 2017.

Lévesque, M., Rigling, A., Bugmann, H., Weber, P., and Brang, P.: Growth response of five co-occurring conifers to drought across a wide climatic gradient in Central Europe, Agric. For. Meteorol., 197, 1–12, 2014.

Maes, W. H., Huete, A. R., Avino, M., Boer, M. M., Dehaan, R., Pendall, E., Griebel, A., and Steppe, K.: Can UAV-based infrared thermography be used to study plant-parasite interactions between mistletoe and eucalypt trees?, Remote Sens., 10, 2062, 2018.

Mamkin, V., Varlagin, A., Yaseneva, I., and Kurbatova, J.: Response of spruce forest ecosystem CO2 fluxes to inter-annual climate anomalies in the Southern Taiga, Forests, 13, 1019, 2022.

Manase, A., Manyevere, A., Abd Elbasit, M. A., and Mashamaite, C.: The use of UAV-based systems in monitoring forest health: potentials and challenges, Sci. Afr., 28, e02724, 2025.

Manrique-Alba, À., Beguería, S., Molina, A. J., González-Sanchis, M., Tomàs-Burguera, M., Del Campo, A. D., Colangelo, M., and Camarero, J. J.: Long-term thinning effects on tree growth, drought response and water use efficiency at two Aleppo pine plantations in Spain, Sci. Total Environ., 728, 138536, 2020.

Matkala, L., Kulmala, L., Kolari, P., Aurela, M., and Bäck, J.: Resilience of subarctic Scots pine and Norway spruce forests to extreme weather events, Agric. For. Meteorol., 296, 108239, 2021.

Martín-Benito, D., Del Río, M., Heinrich, I., Helle, G., and Cañellas, I.: Response of climate-growth relationships and water use efficiency to thinning in a Pinus nigra afforestation, For. Ecol. Manag., 259, 967–975, 2010.

Martínez-García, E., Nilsson, M. B., Laudon, H., Lundmark, T., Fransson, J. E., Wallerman, J., and Peichl, M.: Drought response of the boreal forest carbon sink is driven by understorey–tree composition, Nat. Geosci., 17, 197–204, 2024.

McGloin, R., Šigut, L., Fischer, M., Foltýnová, L., Chawla, S., Trnka, M., Pavelka, M., and Marek, M. V.: Available energy partitioning during drought at two Norway spruce forests and a European beech forest in Central Europe, J. Geophys. Res.-Atmos., 124, 3726–3742, 2019.

McKee, T. B., Doesken, N. J., and Kleist, J.: The relationship of drought frequency and duration to time scales, in: Proceedings of the 8th Conference on Applied Climatology, Vol. 17, No. 22, 179–183, 1993.

Menberu, M. W., Marttila, H., Ronkanen, A.-K., Haghighi, A. T., and Kløve, B.: Hydraulic and physical properties of managed and intact peatlands: application of the van Genuchten–Mualem models to peat soils, Water Resour. Res., 57, e2020WR028624, 2021.

Mirabel, A., Girardin, M. P., Metsaranta, J., Way, D., and Reich, P. B.: Increasing atmospheric dryness reduces boreal forest tree growth, Nat. Commun., 14, 6901, 2023.

Misson, L., Nicault, A., and Guiot, J.: Effects of different thinning intensities on drought response in Norway spruce (Picea abies (L.) Karst.), For. Ecol. Manag., 183, 47–60, 2003.

https://doi.org/10.5194/egusphere-2026-568
Preprint. Discussion started: 5 February 2026

Mohan, M., Silva, C. A., Klauberg, C., Jat, P., Catts, G., Cardil, A., Hudak, A. T., and Dia, M.: Individual tree detection from unmanned aerial vehicle (UAV) derived canopy height model in an open canopy mixed conifer forest, Forests, 8, 340, 2017.

Oogathoo, S., Houle, D., Duchesne, L., and Kneeshaw, D.: Vapour pressure deficit and solar radiation are the major drivers of transpiration of balsam fir and black spruce tree species in humid boreal regions, even during a short-term drought, Agric. For. Meteorol., 291, 108063, 2020.

Ovenden, T. S., Perks, M. P., Clarke, T. K., Mencuccini, M., and Jump, A. S.: Life after recovery: increased resolution of forest resilience assessment sheds new light on post-drought compensatory growth and recovery dynamics, J. Ecol., 109, 3157–3170, 2021.

Owen, P. R. and Thomson, W. R.: Heat transfer across rough surfaces, J. Fluid Mech., 15, 321–334, 1963.

Paulo, A. A., Rosa, R. D., and Pereira, L. S.: Climate trends and behaviour of drought indices based on precipitation and evapotranspiration in Portugal, Nat. Hazards Earth Syst. Sci., 12, 1481–1491, 2012.

Peltoniemi, M.: Dendrometer and sapflow measurements of Norway spruce trees in a peatland harvesting experiment in Ränskälänkorpi, Zenodo, https://doi.org/10.5281/zenodo.10043607, 2023.

Peltoniemi, M.: Temperature invariant tree dendrometer frame – construction and installation, Zenodo, https://doi.org/10.5281/zenodo.18019069, 2025.

Popescu, S. C. and Wynne, R. H.: Seeing the trees in the forest, Photogramm. Eng. Remote Sens., 70, 589–604, 2004.

Pretzsch, H.: Stand density and growth of Norway spruce (Picea abies (L.) Karst.) and European beech (Fagus sylvatica L.): evidence from long-term experimental plots, Eur. J. For. Res., 124, 193–205, 2005.

Pretzsch, H., Schütze, G., and Biber, P.: Drought can favour the growth of small in relation to tall trees in mature stands of Norway spruce and European beech, For. Ecosyst., 5, 1–19, 2018.

Rebmann, C., Aubinet, M., Schmid, H., Arriga, N., Aurela, M., Burba, G., Clement, R., De Ligne, A., Fratini, G., Gielen, B., and Grace, J.: ICOS eddy covariance flux-station site setup: a review, Int. Agrophys., 32, 471–494, 2018.

Rebmann, J., Kučera, J., Bauerle, W. L., Phillips, N., and Hinckley, T. M.: Tree water storage and its diurnal dynamics related to sap flow and changes in stem volume in old-growth Douglas-fir trees, Tree Physiol., 27, 181–198, 2007.

Ruosteenoja, K. and Jylhä, K.: Projected climate change in Finland during the 21st century calculated from CMIP6 model simulations, Geophysica, 56, 39–69, 2021.

Saarinen, N., Vastaranta, M., Näsi, R., Rosnell, T., Hakala, T., Honkavaara, E., Wulder, M. A., Luoma, V., Tommaselli, A. M., Imai, N. N., and Ribeiro, E. A.: Assessing biodiversity in boreal forests with UAV-based photogrammetric point clouds and hyperspectral imaging, Remote Sens., 10, 338, 2018.

Salminen, H. and Jalkanen, R.: Modelling the effect of temperature on height increment of Scots pine at high latitudes, 2005.

Scherrer, D., Bader, M. K. F., and Körner, C.: Drought-sensitivity ranking of deciduous tree species based on thermal imaging of forest canopies, Agric. For. Meteorol., 151, 1632–1640, 2011.

Schmied, G., Hilmers, T., Mellert, K. H., Uhl, E., Buness, V., Ambs, D., Steckel, M., Biber, P., Šeho, M., Hoffmann, Y. D., and Pretzsch, H.: Nutrient regime modulates drought response patterns of three temperate tree species, Sci. Total Environ., 868, 161601, 2023.

https://doi.org/10.5194/egusphere-2026-568
Preprint. Discussion started: 5 February 2026

Schmied, G., Hilmers, T., Uhl, E., and Pretzsch, H.: The past matters: previous management strategies modulate current growth and drought responses of Norway spruce (Picea abies H. Karst.), Forests, 13, 243, 2022.

Schönbeck, L. C., Schuler, P., Lehmann, M. M., Mas, E., Mekarni, L., Pivovaroff, A. L., Turberg, P., and Grossiord, C.: Increasing temperature and vapour pressure deficit lead to hydraulic damages in the absence of soil drought, Plant Cell Environ., 45, 3275–3289, 2022.

Silva, C. A., Hudak, A. T., Vierling, L. A., Loudermilk, E. L., O'Brien, J. J., Hiers, J. K., Jack, S. B., Gonzalez-Benecke, C., Lee, H., Falkowski, M. J., and Khosravipour, A.: Imputation of individual longleaf pine (Pinus palustris Mill.) tree attributes from field and LiDAR data, Can. J. Remote Sens., 42, 554–573, 2016.

Smigaj, M., Agarwal, A., Bartholomeus, H., Decuyper, M., Elsherif, A., de Jonge, A., and Kooistra, L.: Thermal infrared remote sensing of stress responses in forest environments: a review of developments, challenges, and opportunities, Curr. For. Rep., 10, 56–76, 2024.

Sohn, J. A., Saha, S., and Bauhus, J.: Potential of forest thinning to mitigate drought stress: a meta-analysis, For. Ecol. Manag., 380, 261–273, 2016.

Sohn, J. A., Gebhardt, T., Ammer, C., Bauhus, J., Häberle, K.-H., Matyssek, R., and Grams, T. E. E.: Mitigation of drought by thinning: short-term and long-term effects on growth and physiological performance of Norway spruce (Picea abies), For. Ecol. Manag., 308, 188–197, 2013.

Subke, J. A. and Tenhunen, J. D.: Direct measurements of CO2 flux below a spruce forest canopy, Agric. For. Meteorol., 126, 157–168, 2004.

Tardieu, F. and Simonneau, T.: Variability among species of stomatal control under fluctuating soil water status and evaporative demand: modelling isohydric and anisohydric behaviours, J. Exp. Bot., 419–432, 1998.

Thom, A. S., Stewart, J. B., Oliver, H. R., and Gash, J. H. C.: Comparison of aerodynamic and energy budget estimates of fluxes over a pine forest, Q. J. R. Meteorol. Soc., 101, 93–105, 1975.

Tmušić, G., Manfreda, S., Aasen, H., James, M. R., Gonçalves, G., Ben-Dor, E., Brook, A., Polinova, M., Arranz, J. J., Mészáros, J., and Zhuang, R.: Current practices in UAS-based environmental monitoring, Remote Sens., 12, 1001, 2020.

Tupek, B., Mäkipää, R., Heikkinen, J., Peltoniemi, M., Ukonmaanaho, L., Hokkanen, T., Nöjd, P., Nevalainen, S., Lindgren, M., and Lehtonen, A.: Foliar turnover rates in Finland – comparing estimates from needle-cohort and litterfall-biomass methods, 2015.

Venäläinen, A., Lehtonen, I., Laapas, M., Ruosteenoja, K., Tikkanen, O. P., Viiri, H., Ikonen, V. P., and Peltola, H.: Climate change induces multiple risks to boreal forests and forestry in Finland: a literature review, Glob. Change Biol., 26, 4178–4196, 2020.

Verma, S. B.: Aerodynamic resistances to transfers of heat, mass and momentum, Papers in Natural Resources, 1211, 1989.

Vicca, S., Balzarolo, M., Filella, I., Granier, A., Herbst, M., Knohl, A., Longdoz, B., Mund, M., Nagy, Z., Pintér, K., and Rambal, S.: Remotely-sensed detection of effects of extreme droughts on gross primary production, Sci. Rep., 6, 28269, 2016.

Vicente-Serrano, S. M., Beguería, S., and López-Moreno, J. I.: A multiscalar drought index sensitive to global warming: the standardized precipitation evapotranspiration index, J. Clim., 23, 1696–1718, 2010.

https://doi.org/10.5194/egusphere-2026-568
Preprint. Discussion started: 5 February 2026

Vitali, V., Büntgen, U., and Bauhus, J.: Silver fir and Douglas fir are more tolerant to extreme droughts than Norway spruce in south-western Germany, Glob. Change Biol., 23, 5108–5119, 2017.

Wallin, G., Linder, S., Lindroth, A., Räntfors, M., Flemberg, S., and Grelle, A.: Carbon dioxide exchange in Norway spruce at the shoot, tree and ecosystem scale, Tree Physiol., 21, 969–976, 2001.

Wang, J., Taylor, A. R., and D'Orangeville, L.: Warming-induced tree growth may help offset increasing disturbance across the Canadian boreal forest, Proc. Natl. Acad. Sci. USA, 120, e2212780120, 2023.

Waring, R. H. and Franklin, J. F.: Evergreen coniferous forests of the Pacific Northwest: massive long-lived conifers dominating these forests are adapted to a winter-wet, summer-dry environment, Science, 204, 1380–1386, 1979.

Zang, C., Pretzsch, H., and Rothe, A.: Size-dependent responses to summer drought in Scots pine, Norway spruce and common oak, Trees, 26, 557–569, 2012.

Zang, C. S., Buras, A., Esquivel-Muelbert, A., Jump, A. S., Rigling, A., and Rammig, A.: Standardized drought indices in ecological research: why one size does not fit all, Glob. Change Biol., 26, 322–324, 2020.

Zavadilová, I., Szatniewska, J., Stojanović, M., Fleischer, P., Vágner, L., Pavelka, M., and Petrík, P.: The effect of thinning intensity on sap flow and growth of Norway spruce, J. For. Sci., 69, 205–216, 2023.

Zhao, J., Lange, H., and Meissner, H.: Estimating carbon sink strength of Norway spruce forests using machine learning, Forests, 13, 1721, https://doi.org/10.3390/f13101721, 2022.

Zhong, Z., He, B., Wang, Y. P., Chen, H. W., Chen, D., Fu, Y. H., Chen, Y., Guo, L., Deng, Y., Huang, L., and Yuan, W.: Disentangling the effects of vapor pressure deficit on northern terrestrial vegetation productivity, Sci. Adv., 9, eadf3166, 2023.

Zlobin, I. E., Kartashov, A. V., Pashkovskiy, P. P., Ivanov, Y. V., Kreslavski, V. D., and Kuznetsov, V. V.: Comparative photosynthetic responses of Norway spruce and Scots pine seedlings to prolonged water deficiency, J. Photochem. Photobiol. B, 201, 111659, 2019.

Zweifel, R., Item, H., and Häsler, R.: Link between diurnal stem radius changes and tree water relations, Tree Physiol., 21, 869–876, 2001.

Zweifel, R., Zimmermann, L., and Newbery, D. M.: Modeling tree water deficit from microclimate: an approach to quantifying drought stress, Tree Physiol., 25, 147–156, 2005.